

# Journal of Visualized Experiments

## Oligomerization dynamics of membrane receptors in living cells by Total Internal Reflection Fluorescence Microscopy and Number and Brightness analysis --Manuscript Draft--

<b>Article Type:</b>	Methods Article - JoVE Produced Video
<b>Manuscript Number:</b>	JoVE60398R1
<b>Full Title:</b>	Oligomerization dynamics of membrane receptors in living cells by Total Internal Reflection Fluorescence Microscopy and Number and Brightness analysis
<b>Section/Category:</b>	JoVE Biology
<b>Keywords:</b>	Receptor clusters, N&B, Number and Brightness, moment analysis, protein oligomers, cell membrane, TIRF microscopy
<b>Corresponding Author:</b>	Valeria R. Caiolfa Ospedale San Raffaele Milan, Italy ITALY
<b>Corresponding Author's Institution:</b>	Ospedale San Raffaele
<b>Corresponding Author E-Mail:</b>	Valeria.Caiolfa@hsr.it
<b>Order of Authors:</b>	Valeria R. Caiolfa Moreno Zamai Antonio Trullo Elvira Arza Ugo Cavallaro
<b>Additional Information:</b>	
<b>Question</b>	<b>Response</b>
Please indicate whether this article will be Standard Access or Open Access.	Standard Access (US\$2,400)
Please indicate the <b>city, state/province, and country</b> where this article will be <b>filmed</b> . Please do not use abbreviations.	Madrid, Madrid, Spain

**TITLE:**

Oligomerization Dynamics of Cell Surface Receptors in Living Cells by Total Internal Reflection Fluorescence Microscopy Combined with Number and Brightness Analysis

**AUTHORS AND AFFILIATIONS:**

Moreno Zamai<sup>1,#</sup>, Antonio Trullo<sup>2,\*</sup>, Elvira Arza<sup>1</sup>, Ugo Cavallaro<sup>3</sup>, Valeria R. Caiolfa<sup>1,2,#</sup>

1. Unit of Microscopy and Dynamic Imaging, Centro Nacional de Investigaciones Cardiovasculares (CNIC), Madrid, Spain

2. Centro di Imaging Sperimentale, Ospedale San Raffaele, Milano, Italy

3. Unit of Gynecological Oncology Research, European Institute of Oncology IRCCS, Milan, Italy

\*Present address:

Transcription and Development Group, Institut de Génétique Moléculaire de Montpellier (IGMM) CNRS-UMR, Montpellier, France

#Corresponding authors:

Valeria R. Caiolfa ([valeria.caiolfa@hsr.it](mailto:valeria.caiolfa@hsr.it))

Moreno Zamai ([mzamai@cnic.es](mailto:mzamai@cnic.es))

Email addresses of co-authors:

Antonio Trullo ([antonio.trullo@igmm.cnrs.fr](mailto:antonio.trullo@igmm.cnrs.fr))

Elvira Arza ([earza@cnic.es](mailto:earza@cnic.es))

Ugo Cavallaro ([ugo.cavallaro@ieo.it](mailto:ugo.cavallaro@ieo.it))

**KEYWORDS:**

Receptor clusters, N&B, Number and Brightness, moment analysis, protein oligomers, cell membrane, TIRF microscopy

**SUMMARY:**

We describe an imaging approach for the determination of the average oligomeric state of mEGFP-tagged-receptor oligomers induced by ligand binding in the plasma membrane of living cells. The protocol is based on Total Internal Reflection Fluorescence (TIRF) microscopy combined with Number and Brightness (N&B) analysis.

**ABSTRACT:**

Despite the importance and ubiquity of receptor oligomerization, few methods are applicable for detecting clustering events and measuring the degree of clustering. Here, we describe an imaging approach to determine the average oligomeric state of mEGFP-tagged-receptor homocomplexes in the membrane of living cells. The protocol is based on Total Internal Reflection Fluorescence (TIRF) microscopy combined with Number and Brightness (N&B) analysis. N&B is a method similar to fluorescence-correlation spectroscopy (FCS) and photon counting histogram (PCH), which are based on the statistical analysis of the fluctuations of the

fluorescence intensity of fluorophores diffusing in and out of an illumination volume during an observation time. In particular, N&B is a simplification of PCH to obtain information on the average number of proteins in oligomeric mixtures. The intensity fluctuation amplitudes are described by the molecular brightness of the fluorophore and the average number of fluorophores within the illumination volume. Thus, N&B considers only the first and second moments of the amplitude distribution, namely, the mean intensity and the variance. This is, at the same time, the strength and the weakness of the method. Because only two moments are considered, N&B cannot determine the molar fraction of unknown oligomers in a mixture, but it only estimates the average oligomerization state of the mixture. Nevertheless, it can be applied to relatively small time series (compared to other moment methods) of images of live cells on a pixel-by-pixel basis, simply by monitoring the time fluctuations of the fluorescence intensity. It reduces the effective time-per-pixel to a few microseconds, allowing acquisition in the time range of seconds to milliseconds, which is necessary for fast oligomerization kinetics. Finally, large cell areas as well as sub-cellular compartments can be explored.

## INTRODUCTION

We describe a Total Internal Reflection Fluorescence-Number and Brightness (TIRF-N&B) imaging approach for determining the average oligomeric state of receptor molecules at the plasma membrane of live cells, aiming at linking the receptor assembly dynamics to the biological function of the proteins (**Figure 1**).

Upon extracellular ligand binding, receptors initiate the intracellular signal transduction depending on their conformation, oligomerization, potential co-receptors and membrane composition. Despite the importance and ubiquity of receptor oligomerization, recognized as a key event in cellular signaling<sup>1-7</sup>, few methods can detect clustering events and measure the degree of clustering experimentally<sup>8,9</sup>. The confocal volume ( $x,y \approx 300$  nm,  $z \approx 900$  nm) is insufficiently resolved for proving molecular interaction and stoichiometry, even after optimization by image restoration algorithms<sup>10</sup>. The sub-unit composition of protein oligomers cannot be resolved on a purely spatial basis even by super-resolution methods at  $x,y$  resolution of 20-70 nm such as PALM<sup>11</sup>, STORM<sup>12</sup>, and STED<sup>13</sup>. Moreover, their temporal resolution (in the order of minutes per image) cannot follow kinetics in the range of seconds. Single molecule step-bleaching resolves the stoichiometry of protein oligomers only if they are immobile<sup>14</sup>.

One of the most versatile methods to measure density and oligomerization of fluorescently tagged proteins within single images is the spatial intensity distribution analysis (SpIDA), which relies on spatial sampling. It is applicable to both chemically fixed and live cells, and allows the analysis of several regions of interest of the cell simultaneously using standard fluorescence microscopy<sup>15</sup>. Alternatively, moment methods, such as fluorescence-correlation spectroscopy (FCS)<sup>16</sup>, photon counting histogram (PCH)<sup>17</sup>, and Number and Brightness (N&B)<sup>18,19</sup>, are suitable for quantitative oligomer measurements. These methods analyze the fluorescence intensity fluctuations that can be observed in time when the fluorophores diffuse in and out of an illumination volume. The amplitudes of the intensity fluctuations can be uniquely described by the molecular brightness of the fluorophore ( $\epsilon$ ) and the average number of fluorophores ( $n$ ) within the illumination volume<sup>17</sup> (**Figure 2**). Typically, the diffusion coefficient of the

fluorophores and the average number of molecules (inversely related to the  $G(0)$  value) within the illumination volume can be obtained by FCS<sup>20</sup>. However, since the diffusion time only scales with the cubic root of the mass, FCS is not sufficiently sensitive to detect changes in molecular mass<sup>21</sup>. In practice, single color FCS cannot detect dimerization of membrane receptors. PCH resolves mixtures of different oligomers accurately. Using more than two moments of the amplitude distribution, it detects molecules of different brightness that occupy the same illumination volume. Scanning FCS<sup>22</sup> and developments, such as the interesting pair-correlation of molecular brightness (pCOMB) approach<sup>23</sup>, introduced to extend the range of applicability of fluorescence correlation methods in biological systems<sup>24</sup>, remain single point methods lacking the capability of fast measurements in a large area of a cell, requiring many consecutive observations at each pixel and data acquisition in the order of seconds.

N&B is a simplified version of PCH that considers only the first and second moments of the amplitude of the fluorescence distribution, namely the mean intensity,  $\langle I \rangle$ , and the variance,  $\sigma^2$  (**Figure 2**)<sup>18,19</sup> and, because of that, it cannot determine the molar fraction of unknown oligomers in a mixture, but only estimates the average oligomerization state of the mixture. Nevertheless, N&B has the advantage of working with relatively smaller time series of images of live cells than PCH on a pixel-by-pixel basis, simply by monitoring the fluctuations on time of the fluorescence intensity. Because N&B reduces the time-per-pixel to a few microseconds, it can follow fast oligomerization kinetics over large cell areas, allowing image acquisition on a time scale of seconds in raster scanning microscopy (e.g., confocal, 2-photon) and milliseconds in camera-based microscopy (e.g., TIRFM).

Several reports have demonstrated the capability of N&B to quantify the number of subunits in protein clusters by imaging extended cell regions. Paxillin-EGFP clusters were detected at the adhesion sites in CHO-K1 cells<sup>25</sup>, and the intracellular aggregation of the pathogenic Httex1p peptide was described in COS-7 cells<sup>26</sup>. N&B was applied for following the ligand-driven oligomerization of the ErbB receptor<sup>27</sup>, and the effect of the ligand FGF21 on Klothob (KLB) and FGFR1c in HeLa cells<sup>28</sup>. The combination of TIRF imaging and N&B analysis was used to show that dynamin-2 is primarily tetrameric throughout the entire cell membrane<sup>29</sup>. We applied N&B to both raster scanning and TIRF images to prove ligand-driven dimerization of uPAR and FGFR1 cell membrane receptors<sup>30,31</sup>.

Fluorescence correlation methods, such as N&B, FCS and PCH, are based on the notion that in an open volume the occupation number of particles follows a Poisson distribution. Because only the photons that the fluorophores emit can be detected, the mean value for a measured fluorescence intensity versus time in a pixel of the image,  $\langle I \rangle$ , is the product of the average number of fluorophores in the illumination volume,  $n$ , and their molecular brightness,  $\varepsilon$ <sup>17</sup>:

$$eq. 1 \quad \langle I \rangle = \varepsilon n$$

where  $\varepsilon$  is expressed as the number of photons emitted per unit of time (conventionally per second) per molecule when the molecule is at the center of the illumination volume.



Brightness is a property of each fluorophore in a given acquisition set up, while intensity is the sum of all contributions from all fluorophores. In biological contests, brightness will increase with the increase of the number of fluorophores that fluctuate together, giving information on the oligomerization state of the fluorescently-tagged protein. The fluctuation amplitudes at a given pixel is measured from the variance of the fluorescence signal,  $\sigma^2$ :

$$eq. 2 \sigma^2 = \langle I^2 \rangle - \langle I \rangle^2$$

Where the mean of the square of intensity,  $\langle I^2 \rangle$ , and the square of the mean of intensity,  $\langle I \rangle^2$ , are computed from the individual intensity values in each pixel of each frame:

$$eq. 3 \frac{I_1 + I_2 + I_3 + \dots I_K}{K} = \langle I \rangle$$

$$eq. 4 \frac{I_1^2 + I_2^2 + I_3^2 \dots I_K^2}{K} = \langle I^2 \rangle$$

where  $K$  is the number of total frames in the time series. Experimentally, it is necessary to compute for the entire image series the variance that describes the scatter of the individual intensity values at each pixel of a single image around the mean intensity value. The variance includes all fluctuations of different origins. In a first approximation, the variance due the diffusing particles in the illumination volume,  $\sigma_0^2$ , can be separated from the variance due to the detector shot noise,  $\sigma_d^2$ . The two variances are independent; thus, the total variance is given by their sum:

$$eq. 5 \sigma^2 = \sigma_0^2 + \sigma_d^2$$

The variance, due to molecular fluctuations in and out of the detection volume, is linearly dependent on the molecular brightness and intensity:

$$eq. 6 \sigma_0^2 = \varepsilon \langle I \rangle$$

Rearranging eq. 6 according to eq. 1:

$$eq. 7 \sigma_0^2 = \varepsilon^2 n$$

According to the typical concept in fluorescence correlation spectroscopy, equation 7 states that the variance due to the number of fluctuations depends on the square of the particle brightness.

Then, the variance due to detector fluctuations is a linear function of the detected intensity, under the assumption that the detector is operated below its saturation limit<sup>19</sup>:

$$eq. 8 \sigma_d^2 = a \langle I \rangle + c$$

In the case of photon counting detectors  $a=1$  and  $c=0$ , thus the detector variance is equal to the average intensity:

$$eq. 9 \sigma_d^2 = \langle I \rangle$$

To apply these concepts to real measurements in live cells, Gratton and colleagues<sup>18</sup> define the apparent brightness,  $B$ , for each pixel as the ratio of the variance over the average intensity:

$$eq. 10 B = \frac{\sigma^2}{\langle I \rangle} = \frac{\sigma_0^2}{\langle I \rangle} + \frac{\sigma_d^2}{\langle I \rangle} = \frac{\varepsilon^2}{\varepsilon n} + \frac{\varepsilon n}{\varepsilon n} = \varepsilon + 1$$

$B$  is the parameter that is measured experimentally. In this work, time series images of FGFR1 receptors at the plasma membrane of HeLa cells are captured by TIRF microscopy and the average apparent brightness,  $B$ , is determined by the N&B analysis. Then, after addition of FGF2, consecutive time series are captured to follow the changes in the self-assembly of the receptor molecules in the membrane surface after stimulation of the receptor with the canonical ligand.

However, since the detector of the TIRF microscope is a EMCCD camera, the expression for the apparent brightness needs to be modified as<sup>19</sup>:

$$eq. 11 B = \frac{\sigma^2 - \sigma_d^2}{(\langle I \rangle - offset)}$$

where *offset* is the intensity offset of the detection electronics that is a characteristic of the detector settings. The variance and average intensity for an analog detector are respectively given by:

$$eq. 12 \sigma^2 - \sigma_d^2 = SG\varepsilon n + G^2\gamma\varepsilon^2 n$$

$$eq. 13 \langle I \rangle - offset = G\varepsilon n$$

where  $G$  is the analog gain in digital levels (DL/photons),  $S$ , the digital levels per photon<sup>19</sup>, is given by the slope of an intensity versus variance plot for a light source with constant intensity (no temporal fluctuations). The  $\gamma$  factor is related to the shape of the pixel detection volume. According to Hassler et al.<sup>32</sup>, the  $\gamma$  factor is equal to 0.3 for TIRF imaging working at the maximum gain of the detection camera<sup>19</sup>. The offset,  $S$  and  $G$  parameters are characteristics of the camera and the microscope. The apparent brightness,  $B$ , is obtained by rearranging eq. 11 according to eq. 12 and 13:

$$eq. 14 \frac{B}{S} = \frac{G}{S}\gamma\varepsilon + 1$$

Experimentally,  $\varepsilon$  is a complex function of laser intensity and the detection efficiency of the system. Nevertheless, since  $B/S$  is linearly dependent on  $\varepsilon$ , it is only important to determine the relative value of  $\varepsilon$  for a given detection mode:

$$eq. 15 \quad \frac{B}{S} = B' = \varepsilon' + 1$$

where  $\varepsilon'$  is proportional to  $\varepsilon$ . Still, a calibration is performed using an internal reference.

## PROTOCOL

### 1. Sample preparation

1.1. Day 1. Seed HeLa cells in complete medium at a concentration of 100,000-200,000 cell/mL in glass-bottom dishes. Seed 6-8 replicate dishes.

NOTE: In this example, the medium is supplemented with 10% heat inactivated Fetal Bovine Serum (FBS), 1 mM sodium pyruvate, 100 U/100  $\mu$ g penicillin/streptomycin. Several replicate dishes are prepared.

1.2. Day 2-3. When cells are at sub-confluency, transfect half of the dishes with the protein plasmid and the second half with reference plasmids (monomer and dimer), in serum-free medium.

NOTE: Transfection is made in serum free medium supplemented with antibiotics, 0.1% Bovine Serum Albumin and 25 mM HEPES buffer, without Phenol Red.

1.3. Day 3-4. Check that the transfected cells are adherent to the bottom of the dishes and the cell membrane is fluorescent. Discard dishes with overgrown cells or with very low fluorescence.

NOTE: Do not let cells overgrow. Cells must be well distributed and be adhered to the glass area of the dish (**Figure 1A**). Precoated glass bottom dishes can be used for favoring cell adhesion. The cell culture is tested for mycoplasma contamination before any experiment. In this example, cells are transfected with a (A207K)mEGFP-FGFR1 plasmid and the reference cells are transfected with a GPI-(A207K)mEGFP and a GPI-(A207K)mEGFP-(A207K)mEGFP plasmids using standard protocols. For live cell microscopy, an indicator-free medium is recommended; 25 mM HEPES buffer is added to prevent pH changes during imaging.

### 2. TIRF imaging - alignment of the laser line and optimization of TIRF illumination

2.1. Four hours before experiment, activate the temperature incubator of the microscope at 37 °C.

2.2. Turn on the microscope, computers and cameras and wait for the cameras to reach the proper working temperature.

NOTE: The working temperature of the camera used in this study is -70 °C.

2.3. Place a little drop of oil on the objective. Put a sample dish in place. Close the doors of the incubator and let the temperature of the dish equilibrate (~10 min).

2.4. Turn on the epifluorescence lamp and the 488 nm laser.

2.5. Select the epifluorescence contrast mode to explore the sample, searching a cell to focus from the ocular.

NOTE: The use of a fluorescent lamp for searching cells through the ocular is not mandatory. A suitable laser line can be used instead.

2.6. Select the proper filter for collecting the green emission through the microscope camera (Band Pass Ex 490/20 (500) Band Pass Em 525/50, or similar).

2.7. Switch from the ocular to the camera port (camera #1 in **Figure 1**) in epifluorescence mode, refine the focus and change to TIRF mode. Epifluorescence and TIRF modes might be named with a different nomenclature depending on the brand of the microscope.

NOTE: There may be issues focusing or aligning the laser if there are no fluorescent markers at the coverslip interface. To align the laser properly (essential for good TIRF), focus on the coverslip. It is often very difficult to determine whether the coverslip is in focus. As a suggestion, focus on the edges of the cells.

2.8. Activate the auto-alignment following the instructions of the TIRF microscope.

NOTE: Briefly, for steps from 2.4 to 2.8, first find the cells through the ocular and focus on them, then send the emission to the camera port of the TIRF microscope, re-focus the cells on the microscope computer screen and activate the procedure for laser alignment. The alignment consists in finding the critical angle at which illumination becomes evanescent (**Figure 3**). Commercial microscopes might have slightly different alignment protocols and also be fully automated; others might have a small camera for facilitating the visualization of the critical angle conditions.

2.9. Choose a suitable illumination depth and optimize the direction of the evanescent field (**Figure 3**).

### 3. TIRF imaging: capture of the time series

3.1. Define a region of interest (ROI) of at least 256 x 256 pixels.

NOTE: In this set up, the capture is done with camera #2 under software that directly controls only the camera (See **Figure 1** legend).

3.2. Set the exposure to 1 ms and the EM gain to 1000 (this is the G factor in eq. 12 and 13). At such a speed, it might be necessary to adjust or increase the laser power. Here laser power is 0.5 mW.

NOTE: Depending on the type of the camera and the limits imposed by the diffusion coefficient of the protein, fluorescence intensity and background, the general criteria for setting the laser power are not to saturate the detector, minimize photobleaching, and capture as fast as possible at a reasonable S/N. The EM gain is always set at the maximum of the camera (see Introduction).

3.3. Run a first trial sequence under initial conditions and roughly estimate the S/N value. The conditions are acceptable at S/N = 2-3 or higher, as measured in the first frame of the first time series.

3.4. Use the slider of the emission splitting system connecting camera #2 to the microscope for masking a side of the image (**Figure 1B, Figure 4A-B**)

NOTE: In this set up a multichannel imaging connector is installed on camera #2 to enable the acquisition of two spatially identical images simultaneously. The system is equipped with slides for mounting different emission filters. One of the sliders mounts a black mask to cover a side of the image. The masked area is used for the internal calibration of each time series, to determine the camera parameters (eq. 12 and eq. 13). In this way there is no need for an independent calibration step and, importantly, calibration is performed in parallel to the capture of each time series. In the absence of this system, the camera can be calibrated applying published protocols<sup>33</sup>.

3.5. Select the camera **file autosave** option.

3.6. Start the acquisition of the image series. Acquire a minimum of 700 frames at a minimum S/N ratio of 2.

NOTE: The number of frames that are necessary for analysis depends on the sample stability to photobleaching and on the dispersion of the data. Therefore, the quality of each time series is assessed during N&B analysis.

3.7. Without taking the dish out of the microscope, add the ligand.

3.8. Select a cell with a bright fluorescence membrane and quickly start the first time series of the kinetic run.

NOTE: If the addition of the ligand is done quickly, this first capture sets the point = 0 time of the ligand kinetics. The software registers the exact time of the capturing.

3.9. Search a second cell and acquire the second time point of the kinetics.

NOTE: Point-visiting routines are available in some microscopes equipped with x,y,z motorized stages. These allow the memorization of multiple positions on the cell dish, and can help in keeping a more constant interval of time between image-series on different cells.

3.10. Capture a new cell for each time point of the kinetic run.

NOTE: After capturing, a cell is partially photobleached and it cannot be re-imaged. Because of that, the kinetics is obtained by combining time series of many cells, each captured at a different time point.

3.11. For each new dish, repeat the protocol from step 2.3 to 3.9.

NOTE: For reference dishes, add a volume of the vehicle (PBS supplemented with 0.01% bovine serum albumin) equivalent to that used for the ligand.

#### 4. Number & Brightness (N&B): quality check of the time series

4.1. Convert and save as .TIFF the files acquired with the camera software (.sif files in this example).

4.2. Import .TIFF files in the analysis software routine by activating the N&B graphical user interface (GUI) MATLAB.

NOTE: A customized Matlab executable N&B routine is used here (N&B analysis at <https://www.cnice.es/en/investigacion/2/1187/tecnologia> ). By opening an imported .TIFF file, the routine generates the average intensity image, the average intensity profile and it allows inspecting the series frame-by-frame (**Supplemental Figure S1**). Other software are available for N&B analysis (e.g., SimFCS software).

4.3. Discard series for which the average intensity profile shows more than 10% photobleaching, and series in which there has been an evident cell membrane distortion or translation during acquisition.

4.4. Crop frames that are evidently out-of-focus.

NOTE: A cropping tool is implemented in the routine to discards single or multiple frames within the image series. This operation is allowed because frame-to-frame time is not critical whereas the pixel dwell time (exposure time) is (see Discussion).

4.5. Keep for the analysis only series with at least 500 time frames.

## 5. Number & Brightness (N&B): determination of the camera parameters (offset, $\sigma$ and S)

5.1. Activate the routine **Calibrate Camera**.

5.2. Select an area of at least 20x50 pixels in the detector noise region (**Figure 4**).

NOTE: The routine originates a histogram of the values (also defined Digital Level, DL) and it returns a logarithm plot of the Frequency versus Digital Levels.

5.3. In the log Frequency versus Digital level plot, move the linear red cursor to delimit the Gaussian and the linear part of the curve.

NOTE: The red cursor divides the two sections of the curve, and activates the routine returning the offset, which is the center of the Gaussian function of the camera response, the  $\sigma$  of the Gaussian fit, and the S factor, which is the slope of the linear part of the camera response (**Figure 4C-D**).

## 6. Number & Brightness (N&B): computation of the B-values in selected region-of-interest (ROI)

6.1. Activate the **B** key.

NOTE: This action generates the average intensity image (**Figure 5**, first column) and the B-image in which each individual B-value is associated to the related pixel in the image (**Supplemental Figure S1**).

6.2. Apply a minimum binning (2 2) to reduce the dispersion of the data and to generate the B-I histogram (**Figure 5**, second column).

NOTE: The B-I histogram represents the distribution of the B-values of all pixels of the image versus the pixel intensity.  $Y = B/S$ ;  $X = (\langle I \rangle - \text{offset})/S$  (**Supplemental Figure S1** and eq. 11 and 15).

6.3. Inspect the B-I histogram using the iterative square cursor.

6.4. Select a square ROI for the analysis (**Figure 5**, third column).

NOTE: The cursor synchronizes a mobile mask on the average intensity image, highlighting the pixels that are selected inside the square cursor area (**Supplemental Figure S1**). By this inspection, it is possible to exclude from the analysis the background and areas with very low intensity.

6.5. Generate the B-map of the selected ROI (**Figure 5**, fourth column).

6.6. Save the ASCII file of the B-values associated to the selection.

6.7. Import the ASCII file in a graphic software to compute the frequency distribution of the data and obtain the average B-value  $\pm$  S.E (**Figure 5**, fifth column).

NOTE: If data are homogeneous, the frequency distribution of the B—values approximates a Gaussian distribution.

6.8. Apply eq. 15 to derive the average brightness  $\langle \varepsilon' \rangle = \langle B' \rangle - 1$  [(counts /molecule) per dwell time] for each cell at each time point of the kinetic run. Normalize the data according to:

$$eq. 16 \quad \frac{\langle \varepsilon'_t \rangle}{\langle \varepsilon'_0 \rangle} = \frac{\langle B'_t \rangle - 1}{\langle B'_0 \rangle - 1}$$

where  $\langle B'_t \rangle$  is the average B-value measured at time "t" after ligand addition, and  $\langle B'_0 \rangle$  is the average B-value measured at the time t=0 (10-20 s after ligand addition).

NOTE: The normalization of the results allows the direct comparison of experiments that are carried out in different days. It compensates for differences in the measured brightness due to laser power and technical fluctuations.

6.9. Plot the Normalized Average Brightness versus acquisition time to build the kinetic run (**Figure 6**).

## REPRESENTATIVE RESULTS

The results for two representative HeLa-mEGFP-FGFR1 cells seeded in the same culture dish are shown in **Figure 5** and supplemental **Table S1**. The two cells were captured at time 0 min (**Figure 5A, top**) and 7 min (**Figure 5A, bottom**) after addition of the FGF2 ligand.

**Figure 5** also shows the results of two representative HeLa cells expressing either the pure monomer, GPI-mEGFP (**Figure 5B, top**), or the covalently linked dimeric fluorophore, GPI-mEGFP-mEGFP (**Figure 5B, bottom**), exposed at the cell membrane and captured under the same experimental conditions.

The average apparent brightness, B, in the HeLa-mEGFP-FGFR1 cells increases from  $1.070 \pm 0.001$  S.E. to  $1.141 \pm 0.001$  S.E., whereas the reference monomeric (**Figure 5B, top**) and dimeric (**Figure 5B, bottom**) samples return B values of  $1.070 \pm 0.001$  S.E. and  $1.141 \pm 0.001$  S.E. respectively. Thus, by comparison, the FGFR1 receptor is present mainly in the monomeric form at the cell membrane surface at start, but it progresses towards a predominant dimeric state upon stimulation with its canonical ligand FGF2. On average then, the prevalent state of the FGFR1 molecules in the two representative cells is clearly different.

By applying the analysis to several cells in the same dish, each one captured at a different time point, the average brightness as a function of time is obtained (**Figure 6A**). The kinetic run in



**Figure 6A** describes a slow process of dimerization that persists for several minutes at the cell surface. The FGF2-induced FGFR1 dimerization and subsequent internalization of the receptor is a well-known mechanism<sup>34</sup>; therefore, the results are in full agreement with the present notion on the FGFR1 signal transduction, and confirm the potentiality of the TIRF-N&B approach for studying the oligomerization of cell membrane proteins up to the determination of subtle monomer-dimer dynamics.

The normalized average brightness analysis of the results is a suitable tool for comparing the effect of different ligands on the same receptor. One example is given in **Figure 6B**. The protocol was repeated using the same standards and stimulating the cells with a non-canonical FGFR1 ligand, NCAM-Fc (50 µg/mL). In this case, the kinetic profile reveals fast and cyclic transitions of the receptor in oligomeric mixtures, which also reaches brightness values above that of the dimer. A normalized average value of 3 is repeatedly observed. However, the limitation of the N&B analysis (only two moments of the intensity fluctuation versus time are considered) does not allow to demonstrate undoubtedly the formation of a trimeric form. The same normalized average brightness could be the result of various combinations of larger oligomers and monomers of the receptor. Yet, the results clearly demonstrate the spatiotemporal differences of the effect of the two ligands on the same receptor.

#### **FIGURE AND TABLE LEGENDS**

##### **Figure 1: Overview of the experimental protocol.**

(A) Cells are plated on glass bottom dishes and transfected with the fluorescently tagged receptor. (B) Time series images are captured on a commercial TIRF microscope equipped with a TIRF 100x1.46 oil objective and incubator chamber. In this commercial setup, the software does not allow the built-in EMCCD camera #1 to work at very short exposure times necessary for acquiring N&B time series. This is an important point since the exposure time limits the range of molecular diffusions that can be captured. The shortest the exposure time, the faster the molecular diffusion that can be analyzed. Exposures ranging from 0.5 to 1 ms are sufficiently fast for membrane protein diffusion. Therefore, a second EMCCD camera (#2) is added to an additional port of the microscope to work directly under the camera software, bypassing the microscope software. In this adapted configuration, the microscope software and camera #1 are used only for TIRF alignment. TIRF time series are then acquired using camera #2 that runs at very short exposure times such as 1 ms and at the maximum EM gain. Camera #2 also has a pixel size of 124 nm that allows oversampling and binning of the images (see protocol section 6.2). Other configurations to gain imaging speed are possible, depending on the characteristics of different TIRF microscopes, whereas the use of sCMOS cameras is not advisable, because noise is not random in the image<sup>35</sup>. (C) After capturing, time series are inspected as a quality check. Series are discarded if photobleaching is higher than 10% as it can be determined by plotting the average frame intensity versus frame number. Series are also discarded if there has been an evident distortion of the cell membrane or translation of the cell during acquisition. (D) The average intensity in each pixel is saved. (E) A B-I histogram representing the apparent brightness, B, in each pixel of the image is generated. (F) The B-I histogram is used for selecting a ROI that is above the background. (G) The frequency distribution of the B-values is analyzed to determine the average B-value  $\pm$  S.E.

**Figure 2: N&B principle.**

N&B quantifies the average oligomerization state of fluorophores by measuring the fluorescence fluctuations that occur when they move in and out the illumination volume during the acquisition of a time stack series of "K" images. The amplitude of the fluctuations is characterized statistically by computing the ratio between variance of the fluctuating signal,  $\sigma^2$ , and mean intensity value,  $\langle I \rangle$ . In the simplest scenario (A), when the illumination volume is empty (i.e., no fluorophores), the ratio describes instrument noise. If the fluorescence signal fluctuates due to mobile fluorophores (B, C), the "extra" variance is directly proportional to the molecular brightness,  $\epsilon$  (detected photon counts per molecule and per second), of the diffusing molecules. In (B), there are 8 monomeric diffusing fluorophores and in (C), the same fluorophores diffuse as 2 tetrameric oligomers. In these two cases, the average intensity is the same, but the standard deviation and brightness are different ( $1\epsilon$ ,  $4\epsilon$ ), because the amplitudes of the fluctuations are different.  $\epsilon = 0$  when fluorophores are immobile or absent.

**Figure 3: TIRF microscopy.**

Although N&B runs equally well with raster scanning microscopes equipped with multiphoton, continuous wave or pulsed single photon lasers and analogue or photon counting detectors, TIRF microscopy is ideal for fast temporal imaging of molecular dynamic events occurring at or near the cell surface with speeds, resolution and signal/noise ratio (S/N) that are not possible to achieve by other imaging techniques. (A) TIRF microscopy employs the principle of total internal reflection by which an angled excitation laser light excites only fluorophores that are just underneath a glass-water interface of the coverslip. The laser irradiates the specimen at an angle of incidence greater than or equal to the critical angle of refraction whereas the excitation laser light is totally reflected. The reflection generates a very thin electromagnetic field in the specimen called the evanescent wave. The resulting fluorescent light emitted by the tiny illuminated section of the specimen is collected through a microscope objective placed perpendicularly below to the slide. (B) The panel shows a representative example at a given wavelength of the relative intensity of an evanescent field versus depth, which decreases exponentially with increasing distance from the surface, providing high axial resolution fluorescence images. The lateral resolution is set by the numerical aperture and magnification of the objective and by the pixel size of the detection camera. The cell interior is not illuminated and it does not contribute to the signal with intracellular autofluorescence. Multi-angle TIRF microscopes allow selecting various penetration depths. They provide a scale that depends on the excitation wavelength and usually goes from 70 nm up to 250 nm depth for single color TIRF image. The evanescent illumination depth chosen for this protocol is 110 nm, and it is the result of a compromise between the necessity of using low laser power and the intensity of the fluorescence signal that decreases sharply with the decrease of the penetration depth. It is important to avoid overly large evanescent fields that can illuminate many intracellular vesicles and intracellular population of fluorophores. Therefore, depending on the type of sample, several penetration depths should be explored, searching for the best combination: high signal-to-noise ratio, low excitation power, short exposure time, short penetration depth. Once this optimization is done, the penetration depth is kept constant for all controls and samples. (C) Representative epifluorescence and TIRF images of a HeLa-GPI-mEGFP cell after software-

guided optimization of the depth and direction of the evanescent field. Multi angle TIRF microscopes also allow to optimize the direction of the evanescent field. This step is recommended for minimizing scattering (i.e., sharp increase of the intensity and less crisp image), and it can be carried out according to the instructions of the specific microscope used. In this protocol the microscope software includes an automatic optimization of the direction of the evanescent field. For manual optimization, refer to published protocols<sup>36,37</sup>. **(D)** Representative cell expressing the mEGFP-FGFR1 construct in epifluorescence and after optimization of the TIRF illumination.

**Figure 4: Capture of the time series and calibration of the camera response to single photons.**

**(A)** Example of the first frame out of 700-frame time series captured on a HeLa-mEGFP-FGFR1 cell in the Cropped Sensor Mode. The camera chip is partially masked (red rectangles) using the dual view connector installed on the TIRF microscope (**Figure 1B**). The internal calibration regions are recognized in the average intensity image **(B)** and processed **(C)** for estimating the camera parameters by plotting the log-frequency versus Digital Levels **(D)**. An analog detection system, such as an EMCCD camera, detects pulses of photocurrent instead of photon counts, and the photon pulse height distribution is quasi-exponential. The first part of the distribution is due to the amplifier and analog-to-digital converter and it contributes a Gaussian readout noise (the variance introduced by the signal recording). The most populated channel (i.e., the most frequent value) of the distribution is the *offset* (eq. 13). Using a vertical cursor in a log plot, the first part of the distribution is separated from the exponential second part, above 250 DL, which represents the average camera response to a single photon (the slope is the S factor in eq. 12). The measurement of these parameters allows estimating the density of photons that are recorded during the acquisition. Counts (DL) are in pseudo color scale. Pixel size = 124 nm; Image format = 256x256 pixels, penetration depth of the evanescent field ~ 110 nm; Calibration ROI #1 = 19x256 pixels; Calibration ROI #2 = 5x256 pixels. DL = digital levels. Exposure = 1 ms and EMGain (the G factor in eq. 12, 13 and 14) = 1000. Note that cameras working in photon counting mode with background are equivalent to analog detectors with  $S = 1$  (eq. 12) and with  $\sigma_d^2$  and offset (eq. 13) measured in the same way as for an analog system<sup>18</sup>.

**Figure 5: N&B analysis of FGFR1 oligomerization.**

**(A)** Representative results from two HeLa cells in the same dish expressing mEGFP-FGFR1 and captured at time 0' (top) and 7' (bottom) after addition of 20 ng/mL FGF2, and **(B)** two HeLa cells expressing the reference constructs GPI-mEGFP (top) and GPI-mEGFP-mEGFP (bottom). The entire analysis sequence shows (from left to right): Average intensity of the time series; Plot of all B-values as a function of fluorescence intensity in which the color code represents the number of pixels having the same B-value in the image and the rectangular cursors delimit the region of interest (ROI), the background (BG) and regions of very low intensity (LI). Notice that immobile fluorophores will give B-value = 1 since in the absence of fluctuations  $\varepsilon = 0$ ; B-map of the chosen ROI and the associated B-distribution histogram. The B-value distribution is fitted with a Gaussian function (dashed red line) to compute the average apparent brightness, B (full red line) and the distribution statistics (supplemental Table S1) B-value =  $B' = B/S$  (eq. 15); Intensity =  $(\langle I \rangle - offset)/S$ ; M = monomer; D = dimer; scale bars = 10 microns. Raw data time

series in **Supplemental Movie 1**, **Supplemental Movie 2**, **Supplemental Movie 3**, and **Supplemental Movie 4**.

**Figure 6: Kinetics of FGFR1 oligomerization induced by ligand activation.**

Representative kinetic runs described by the Normalized Average Brightness (eq. 16) of HeLa-mEGFP-FGFR1 cells after stimulation with 20 ng/mL FGF2 (**A**) or 50 µg/mL NCAM-Fc (**B**). Cells in the same dish were captured at increasing time points and the apparent average brightness,  $B \pm$  S.E., was computed from the B-distribution histograms. The figure is adapted with permission from Zamai et al. Journal of Cell Science (2019)<sup>31</sup>.

**Figure 7: Fast Kinetics and data interpretation.**

Scatter plot of the all Normalized Average Brightness values obtained from replicate kinetic runs in which HeLa-mEGFP-FGFR1 cells were stimulated either with NCAM-Fc (50 µg/mL) or FGF2 (20 ng/mL).

**Supplemental Figure S1: Screen snapshot of the analysis routine in MatLab**

Screen snapshot of the N&B graphical user interface (GUI) MATLAB routine showing the initial analysis steps: upload time series; compute average intensity image, compute intensity profile, compute B-map and B-I histogram.

**Supplemental Table S1: Apparent Brightness Analysis**

Statistics and Gaussian fitting parameters of the B-distributions in **Figure 5** were carried out. The least square Gaussian fits were obtained under the constrain of standard deviation > 0 with the X-range automatically chosen and maximum iterations = 1000. R square: mEGFP-FGFR1 monomer = 0.9957, mEGFP-FGFR1 dimer 0.9940; GPI-mEGFP = 0.9985; GPI-mEGFP-mEGFP = 0.9970.

**Supplemental Movie 1.** Time series of an HeLa-mEGFP-FGFR1 cell at time = 0 minutes after FGF2 stimulation (20 ng/mL in PBS supplemented with 0.01% BSA) shown in **Figure 5**. The series of 800 frames are reproduced uncompressed at 7 fps. Image format = 256x256 pixels; pixel size = 124 nm; The internal calibration area is identified as dark lateral bands.

**Supplemental Movie 2.** Time series shown in **Figure 5** of a HeLa-mEGFP-FGFR1 cell at time = 7 minutes after FGF2 stimulation (20 ng/mL in PBS supplemented with 0.01% BSA) The series of 800 frames are reproduced uncompressed at 7 fps. Image format = 256x256 pixels; pixel size = 124 nm; The internal calibration area is identified as dark lateral bands.

**Supplemental Movie 3.** Time series shown in **Figure 5** of a HeLa-GPI-mEGFP cell after adding the vehicle (PBS supplemented with 0.01% BSA). The series of 1000 frames are reproduced uncompressed at 7 fps. Image format = 256x256 pixels; pixel size = 124 nm; The internal calibration area is identified as dark lateral bands.

**Supplemental Movie 4.** Time series shown in **Figure 5** of a HeLa-GPI-mEGFP-mEGFP cell after adding the vehicle (PBS supplemented with 0.01% BSA). The series of 1000 frames are

reproduced uncompressed at 7 fps. Image format = 256x256 pixels; pixel size = 124 nm; The internal calibration area is identified as dark lateral bands.

## DISCUSSION:

N&B requires several precautions in the choice of the cell model and labelling strategy. It can be applied only to live cells that remain stably adhered during the image capture time. Extra fluctuations due to the whole cell rigid displacement might be handled with appropriate image restoration approaches<sup>38</sup>. However, generally when a cell moves, the cell membrane also deforms, and structure deformation, producing large extra variance, introduces serious limitation to the analysis of membrane proteins. In this work, the fluorescent construct is expressed in the HeLa cell line because the constitutive FGFR1 is negligible. The presence of the constitutive protein is a condition to avoid, otherwise mixed populations of fluorescent and non-fluorescent receptor oligomers would likely form. Consequently, the N&B analysis, which is based only on the brightness of the fluorescently-tagged protein population, would return an unreliable estimation of the average oligomeric state. This aspect is particularly important when applying N&B to detect receptor dimerization events in which the brightness only increases by a factor of 2, such as the FGFR1 dimerization in the presence of the FGF2 ligand. In such a case, the presence of mixed dimers can completely hide the dimerization events detectable by N&B. The contamination of fluorescent oligomers with non-fluorescent constitutive forms is one of the potential pitfalls of any approach based on the detection of fluorescence, unless the tagged protein is largely overexpressed. However, oligomerization studies in conditions of protein overexpression raise concerns about their functional significance. Transiently transfected cells will likely have variable levels of fluorescence (i.e. protein concentration) and are useful for testing the independence of the average brightness on the protein concentration, since N&B can be applied to a wide range of concentrations, under the condition of linear response of the detector (see the definition of the brightness, eq. 1).

Another constraint is the stoichiometric labelling of the receptor using a stable fluorophore in live cells. Halo-tags, fluorescent proteins (FP) or other covalent fluorescent tags are suitable labels to obtain an exact number of bound fluorophores per molecule of protein in cell. To reduce the complexity of the N&B analysis, we use either fluorescent proteins or halo-tags yielding a 1-to-1 fluorophore-to-protein labelling. The FP of choice must be monomeric in the mature form, having a negligible self-association tendency that, otherwise, might induce artificial oligomerization of the FP-tagged receptors. In this protocol, we use the (A207K)mEGFP because this single point mutation abolishes the mEGFP self-aggregating tendency as previously shown<sup>31,39,40</sup>. Regardless of the labelling strategy, the fluorescently tagged protein should be checked for the retention of the biological activity in the chosen cell model, as the functionality of the tagged molecules is essential for linking oligomerization events to receptor signaling. In our model, we proved the autophosphorylation of the fluorescent (A207K)mEGFP-FGFR1 after stimulating the transfected cells with the receptor ligand FGF2<sup>31</sup>.

N&B is based on the diffusion of molecules in the illumination volume. In digital camera detection, the exposure time (i.e., the pixel dwell time in analog detection,  $t_{dwell}$ ) must be

short enough that one and only one configuration of particles in the focal volume is captured. This is to say that the probability of a fluorophore entering or exiting the illuminated volume during the exposure time is very small. The exposure time must be shorter than the fluorophore residence time ( $\tau_D$ ) which is the average time that a fluorophore spends in the illuminated volume. Therefore, before starting an N&B experiment, it is necessary to have some notion about the residence time (or the diffusion coefficient) of the target protein, which in a first approximation, depends on subcellular localization and molecular mass. Frame rate is the inverse of the time needed for the camera to acquire an image and then completely read that image out, and it is often, calculated approximately from the total number of pixels and the readout rate, combined with the exposure time. Even though frame rate does not need to be fast, cycle time ( $t_{cycle}$ ), which is the sum of the frame rate and the time to prepare the capture of the next frame, might affect the analysis. These constraints can be generalized as:  $t_{cycle} \gg \tau_D \gg t_{dwell}$ . If the cycle time is too fast, the molecules will not have moved appreciably from one frame to the next in that time, and will appear as immobile ( $B = 1$ ). However, because hundreds of frames are needed for the analysis, cycling is set as fast as possible (increasing or decreasing the image format in number of pixels) to avoid cell displacements and distortion of the cell membrane that would add large extra variance during the series acquisition. In the example of this protocol, the slowest cycle time is 22 ms, so that 500 frames can be acquired in 11 s.

Molecular brightness is not an absolute quantity; It depends on the molecular properties of the fluorophore (cross section and quantum yield), on the experimental set up (detector and optics) as well as on the excitation conditions such as the laser power. Thus, the TIRF-N&B approach yields an apparent brightness and because of that it is fundamental to set up a “reference cell model” that expresses a reference construct with univocal oligomeric state. The reference construct carries the same fluorophore tag of the protein under study [here, the (A207K)mEGFP] and it localizes in the same subcellular compartment (here, the plasma membrane). In this work we use a glycosylphosphatidylinositol (GPI) anchored-(A207K)mEGFP construct that we have repeatedly demonstrated to be a reliable monomeric brightness standard for cell surface receptors labelled with the same fluorophore<sup>30,31</sup>.

One major drawback is the occurrence of fluorophore photobleaching that very likely happens when the same cell is repeatedly exposed to light during a kinetic run, and leads to an underestimation of the oligomerization state. To prevent that, the brightness kinetics is obtained by combining the average brightness of different cells each captured at a different time point (**Figure 6**). This is to say that in a Petri dish each cell is a different time point of the kinetics and a petri dish represents an entire kinetic run.

When the oligomerization dynamics is fast and complex, such as the FGFR1 oligomerization induced by a non-canonical ligand, NCAM<sup>31</sup>, the profile of the normalized average brightness versus time can be variable and unstable (**Figure 6B**). In such a case, reproducibility cannot be determined by reading replicate dishes of cells at precise time points, due to the necessity of moving and focusing on a new cell each time, select a ROI, capture and inspect/discard time series. Thus, reproducibility can be evaluated in terms of kinetic profile similarity and amplitude

of the brightness changes.

An overview of the results is presented in **Figure 7**. The scatter plot illustrates only the average brightness measured in cells of the same dish, neglecting the time of each capture. In this plot the major difference induced by the two ligands on the oligomerization state of the receptor remain evident, although all kinetic information is removed. However, for both set of experiments (FGF2- versus NCAM-induced oligomerization), the conventional approach of determining the mean  $\pm$  S.D. of each run in **Figure 7** would lead to misleading conclusions since the FGFR1 molecules stimulated by FGF2 clearly transit into two well defined states, whereas NCAM induces unstable and cyclic oligomeric FGFR1 mixtures that would not be well represented by a mean  $\pm$  S.D. value.

In summary, from an experimental point of view, N&B requires only access to a microscope equipped with a fast acquisition module and a dedicated software. The protein of interest can be tagged with a variety of monomeric fluorescent proteins or organic fluorophores, but quantitative measurements require several conditions to be fulfilled: stoichiometric labelling, reference brightness standard, detector calibration and no photobleaching. In this context, the N&B approach is a powerful tool to decipher the spatiotemporal oligomerization of proteins in live cells. Furthermore, recent advances in resampling raw data to solve the statistical weighting<sup>41</sup> and combining fluorescence cross-correlation spectroscopy with cross-correlation N&B<sup>42</sup> are refining and improving the applicability of the N&B approach to protein oligomerization and interaction studies.

#### **ACKNOWLEDGMENTS :**

The CNIC is supported by the Ministry of Ciencia, Innovacion y Universidades and the Pro CNIC Foundation, and is a Severo Ochoa Center of Excellence (SEV-2015-0505). UC acknowledges the support from the Associazione Italiana Ricerca sul Cancro, the Association for International Cancer Research (now known as Worldwide Cancer Research), and the Italian Ministry of Health. A.T. acknowledge the “Fondazione Banca del Monte di Lombardia” for partly supporting his work with the PV Fellowship “Progetto Professionalità Ivano Becchi” 2011-2012.

#### **DISCLOSURES:**

The authors have nothing to disclose.

#### **REFERENCES:**

- 1 Agwuegbo, U. C., Jonas, K. C. Molecular and functional insights into gonadotropin hormone receptor dimerization and oligomerization. *Minerva Ginecologica*. **70** (5), 539-548 (2018).
- 2 Ferre, S. et al. G protein-coupled receptor oligomerization revisited: functional and pharmacological perspectives. *Pharmacological Reviews*. **66** (2), 413-434 (2014).
- 3 Marsango, S., Ward, R. J., Alvarez-Curto, E., Milligan, G. Muscarinic receptor oligomerization. *Neuropharmacology*. **136** (Pt C), 401-410 (2018).
- 4 Oishi, A., Cecon, E., Jockers, R. Melatonin Receptor Signaling: Impact of Receptor Oligomerization on Receptor Function. *International Review of Cell and Molecular Biology*. **338**

59-77 (2018).

5 Thelen, M., Munoz, L. M., Rodriguez-Frade, J. M., Mellado, M. Chemokine receptor oligomerization: functional considerations. *Current Opinion in Pharmacology*. **10** (1), 38-43 (2010).

6 Van Craenenbroeck, K. GPCR oligomerization: contribution to receptor biogenesis. *Subcellular Biochemistry*. **63** 43-65 (2012).

7 Wnorowski, A., Jozwiak, K. Homo- and hetero-oligomerization of beta2-adrenergic receptor in receptor trafficking, signaling pathways and receptor pharmacology. *Cell Signaling Technology*. **26** (10), 2259-2265 (2014).

8 Fricke, F., Dietz, M. S., Heilemann, M. Single-molecule methods to study membrane receptor oligomerization. *Chemphyschem*. **16** (4), 713-721 (2015).

9 Vidi, P. A., Ejendal, K. F., Przybyla, J. A., Watts, V. J. Fluorescent protein complementation assays: new tools to study G protein-coupled receptor oligomerization and GPCR-mediated signaling. *Molecular and Cellular Endocrinology*. **331** (2), 185-193 (2011).

10 Trussell, H. J. in *Academic Press Library in Signal Processing* Vol. 4 eds Joel Trussell et al.) 3-9 (Elsevier, 2014).

11 Betzig, E. et al. Imaging intracellular fluorescent proteins at nanometer resolution. *Science*. **313** (5793), 1642-1645 (2006).

12 Rust, M. J., Bates, M., Zhuang, X. Sub-diffraction-limit imaging by stochastic optical reconstruction microscopy (STORM). *Nature Methods*. **3** (10), 793-795 (2006).

13 Nagerl, U. V., Willig, K. I., Hein, B., Hell, S. W., Bonhoeffer, T. Live-cell imaging of dendritic spines by STED microscopy. *Proceedings of the National Academy of Sciences of the United States of America*. **105** (48), 18982-18987 (2008).

14 Tsekouras, K., Custer, T. C., Jashnsaz, H., Walter, N. G., Presse, S. A novel method to accurately locate and count large numbers of steps by photobleaching. *Molecular Biology of the Cell*. **27** (22), 3601-3615 (2016).

15 Godin, A. G. et al. Revealing protein oligomerization and densities in situ using spatial intensity distribution analysis. *Proceedings of the National Academy of Sciences of the United States of America*. **108** (17), 7010-7015 (2011).

16 Qian, H., Elson, E. L. Distribution of molecular aggregation by analysis of fluctuation moments. *Proceedings of the National Academy of Sciences of the United States of America*. **87** (14), 5479-5483 (1990).

17 Chen, Y., Muller, J. D., So, P. T., Gratton, E. The photon counting histogram in fluorescence fluctuation spectroscopy. *Biophysical Journal*. **77** (1), 553-567 (1999).

18 Dalal, R. B., Digman, M. A., Horwitz, A. F., Vetri, V., Gratton, E. Determination of particle number and brightness using a laser scanning confocal microscope operating in the analog mode. *Microscopy Research and Technique*. **71** (1), 69-81 (2008).

19 Unruh, J. R., Gratton, E. Analysis of molecular concentration and brightness from fluorescence fluctuation data with an electron multiplied CCD camera. *Biophysical Journal*. **95** (11), 5385-5398 (2008).

20 Hess, S. T., Huang, S., Heikal, A. A., Webb, W. W. Biological and chemical applications of fluorescence correlation spectroscopy: a review. *Biochemistry*. **41** (3), 697-705 (2002).

21 Muller, J. D., Chen, Y., Gratton, E. Fluorescence correlation spectroscopy. *Methods in Enzymology*. **361** 69-92 (2003).



829 22 Levi, V., Ruan, Q., Kis-Petikova, K., Gratton, E. Scanning FCS, a novel method for three-  
830 dimensional particle tracking. *Biochemical Society Transactions*. **31** (Pt 5), 997-1000 (2003).

831 23 Hinde, E. et al. Quantifying the dynamics of the oligomeric transcription factor STAT3 by  
832 pair correlation of molecular brightness. *Nature Communications*. **7** 11047 (2016).

833 24 Waithe, D. et al. Optimized processing and analysis of conventional confocal microscopy  
834 generated scanning FCS data. *Methods*. **140-141** 62-73 (2018).

835 25 Digman, M. A., Dalal, R., Horwitz, A. F., Gratton, E. Mapping the number of molecules  
836 and brightness in the laser scanning microscope. *Biophysical Journal*. **94** (6), 2320-2332 (2008).

837 26 Ossato, G. et al. A two-step path to inclusion formation of huntingtin peptides revealed  
838 by number and brightness analysis. *Biophysical Journal*. **98** (12), 3078-3085 (2010).

839 27 Nagy, P., Claus, J., Jovin, T. M., Arndt-Jovin, D. J. Distribution of resting and ligand-bound  
840 ErbB1 and ErbB2 receptor tyrosine kinases in living cells using number and brightness analysis.  
841 *Proceedings of the National Academy of Sciences of the United States of America*. **107** (38),  
842 16524-16529 (2010).

843 28 Ming, A. Y. et al. Dynamics and Distribution of Klothobeta (KLB) and fibroblast growth  
844 factor receptor-1 (FGFR1) in living cells reveal the fibroblast growth factor-21 (FGF21)-induced  
845 receptor complex. *Journal of Biological Chemistry*. **287** (24), 19997-20006 (2012).

846 29 Ross, J. A. et al. Oligomerization state of dynamin 2 in cell membranes using TIRF and  
847 number and brightness analysis. *Biophysical Journal*. **100** (3), L15-L17 (2011).

848 30 Hellriegel, C., Caiolfa, V. R., Corti, V., Sidenius, N., Zamai, M. Number and brightness  
849 image analysis reveals ATF-induced dimerization kinetics of uPAR in the cell membrane. *FASEB*  
850 *J.* **25** (9), 2883-2897 (2011).

851 31 Zamai, M. et al. Number and brightness analysis reveals that NCAM and FGF2 elicit  
852 different assembly and dynamics of FGFR1 in live cells. *Journal of Cell Science*. **132** (1) (2019).

853 32 Hassler, K. et al. Total internal reflection fluorescence correlation spectroscopy (TIR-FCS)  
854 with low background and high count-rate per molecule. *Optics Express*. **13** (19), 7415-7423  
855 (2005).

856 33 Di Rienzo, C., Gratton, E., Beltram, F., Cardarelli, F. From fast fluorescence imaging to  
857 molecular diffusion law on live cell membranes in a commercial microscope. *Journal of*  
858 *Visualized Experiments*. 10.3791/51994 (92), e51994 (2014).

859 34 Beenken, A., Mohammadi, M. The FGF family: biology, pathophysiology and therapy.  
860 *Nature Reviews Drug Discovery*. **8** (3), 235-253 (2009).

861 35 Joubert, J., Sharma, D. Light microscopy digital imaging. *Current Protocols in Cytometry*.  
862 **Chapter 2** Unit2 3 (2011).

863 36 Gell, C., Berndt, M., Enderlein, J., Diez, S. TIRF microscopy evanescent field calibration  
864 using tilted fluorescent microtubules. *Journal of Microscopy*. **234** (1), 38-46 (2009).

865 37 Burghardt, T. P. Measuring incidence angle for through-the-objective total internal  
866 reflection fluorescence microscopy. *Journal of Biomedical Optics*. **17** (12), 126007 (2012).

867 38 Trullo, A., Corti, V., Arza, E., Caiolfa, V. R., Zamai, M. Application limits and data  
868 correction in number of molecules and brightness analysis. *Microscopy Research and*  
869 *Technique*. **76** (11), 1135-1146 (2013).

870 39 Caiolfa, V. R. et al. Monomer-dimer dynamics and distribution of GPI-anchored uPAR are  
871 determined by cell surface protein assemblies. *Journal of Cell Biology*. **179** (5), 1067-1082  
872 (2007).

873 40 Campbell, R. E. et al. A monomeric red fluorescent protein. *Proceedings of the National*  
874 *Academy of Sciences of the United States of America*. **99** (12), 7877-7882 (2002).  
875 41 Cutrale, F. et al. Using enhanced number and brightness to measure protein  
876 oligomerization dynamics in live cells. *Nature Protocols*. **14** (2), 616-638 (2019).  
877 42 Dunsing, V., Chiantia, S. A Fluorescence Fluctuation Spectroscopy Assay of Protein-  
878 Protein Interactions at Cell-Cell Contacts. *Journal of Visualized Experiments*. (142) (2018).  
879

Figure 1

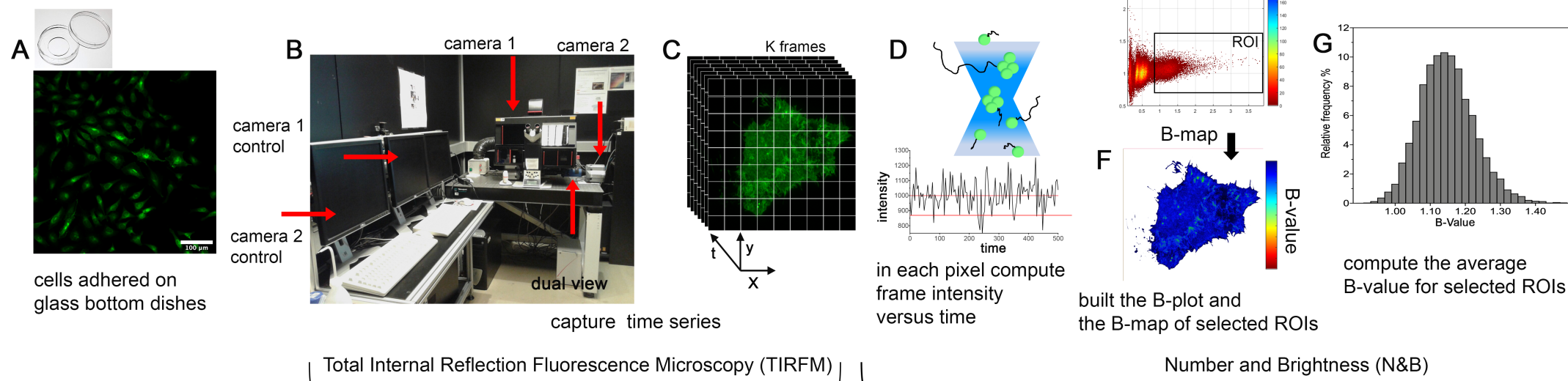


Figure 2

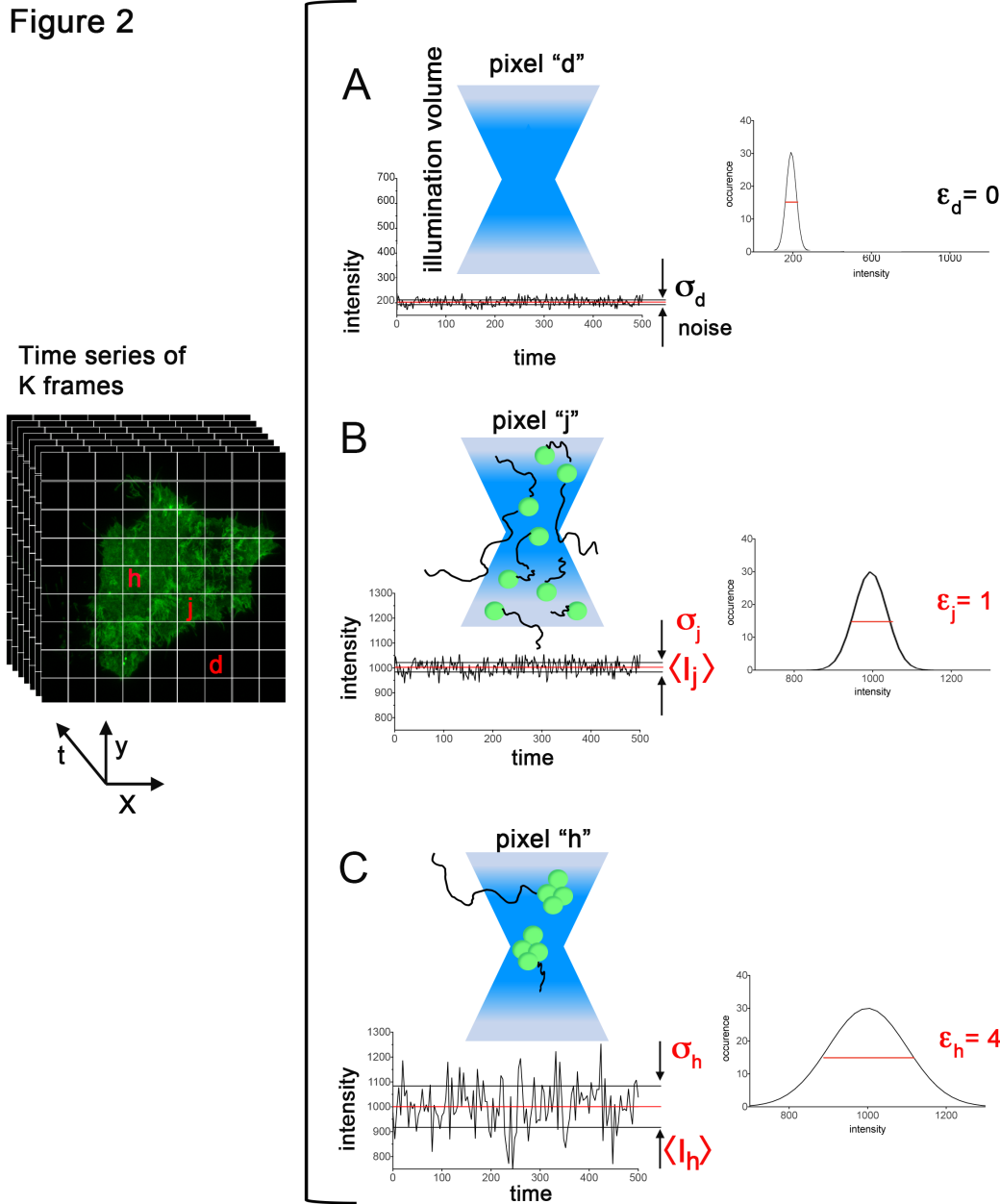


Figure 3

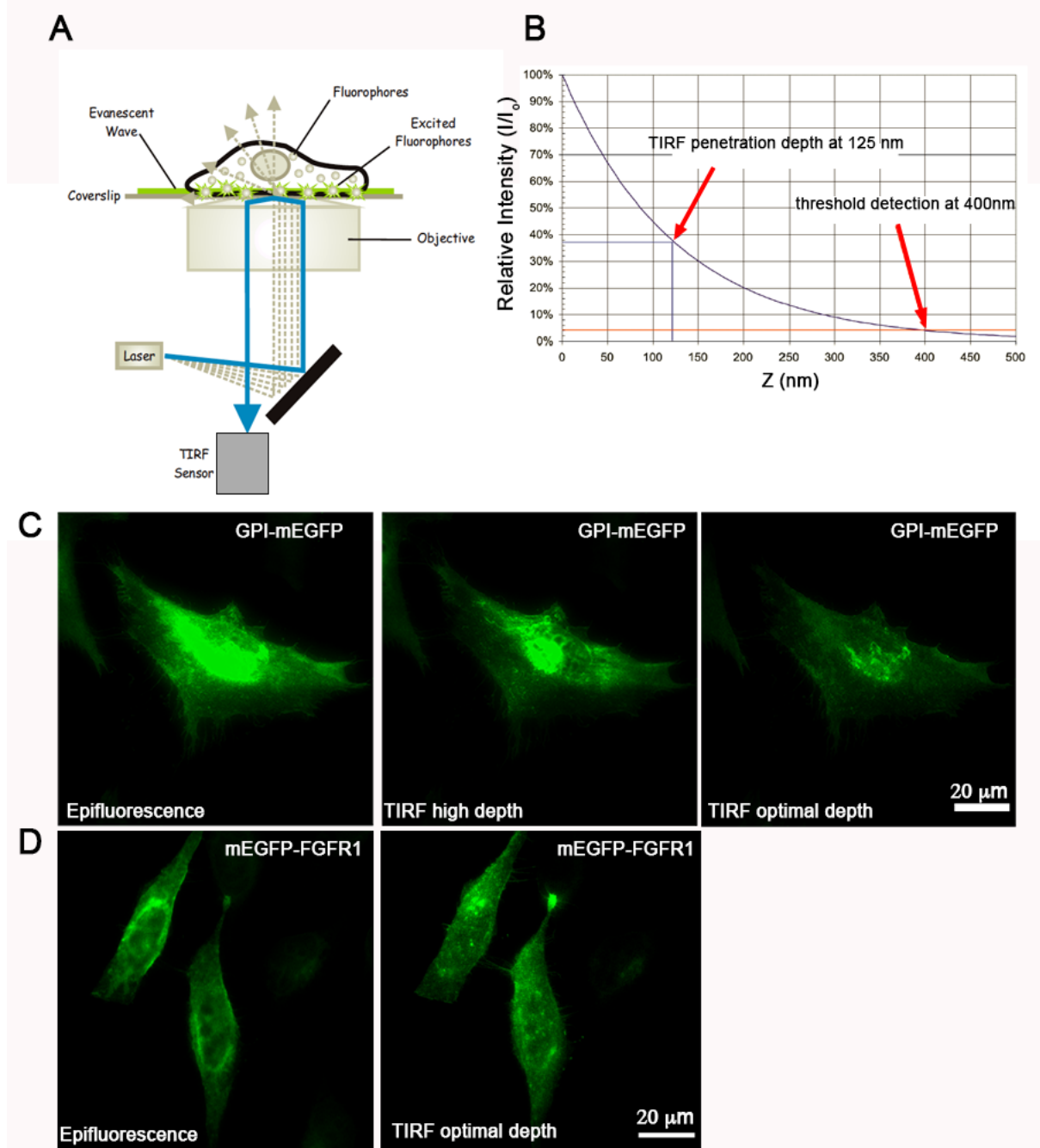


Figure 4

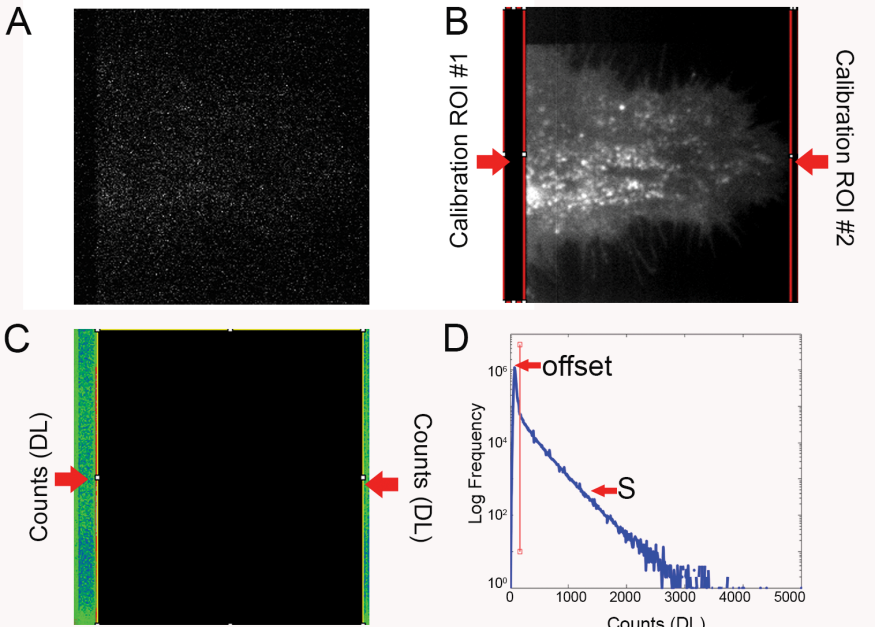


Figure 5

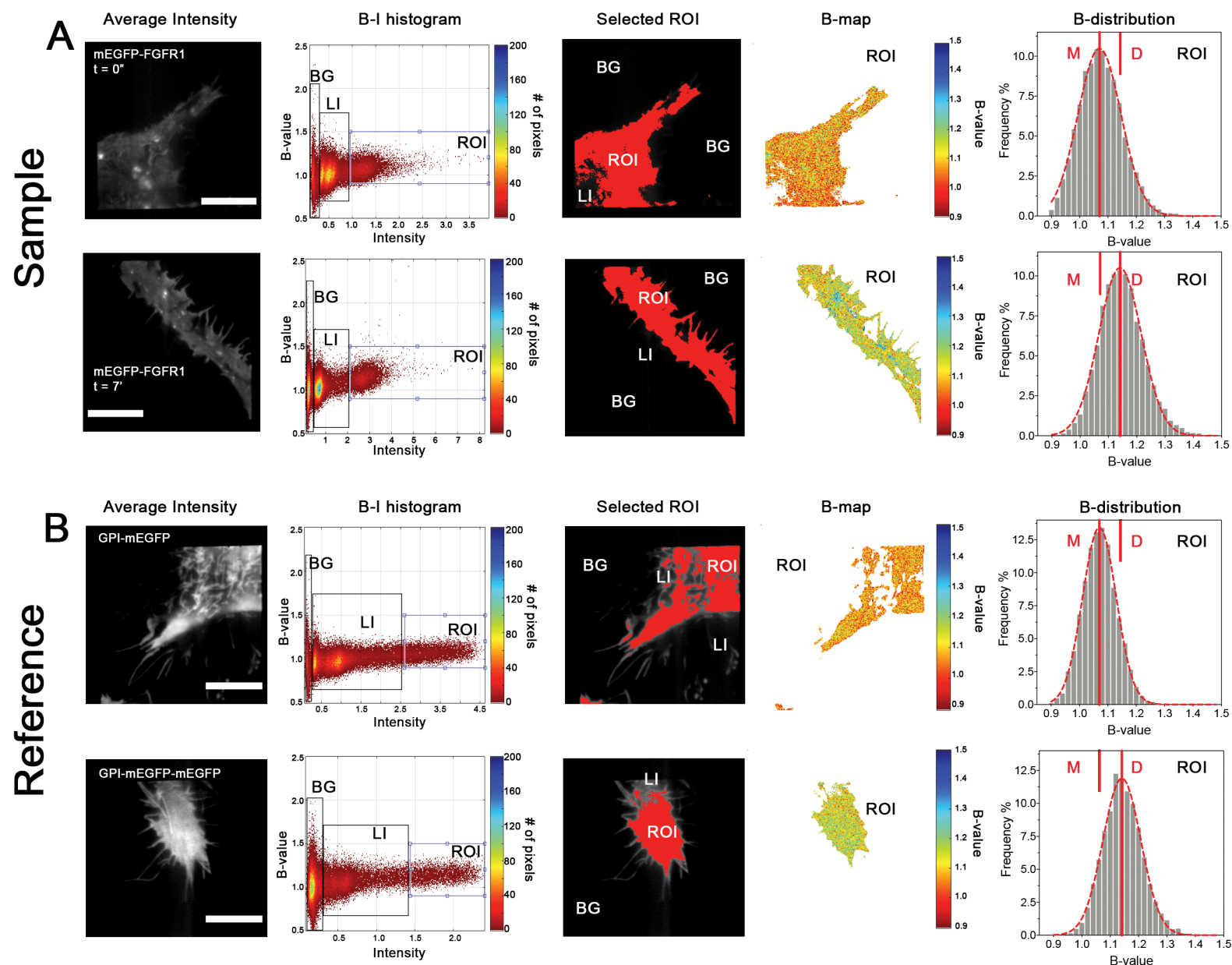
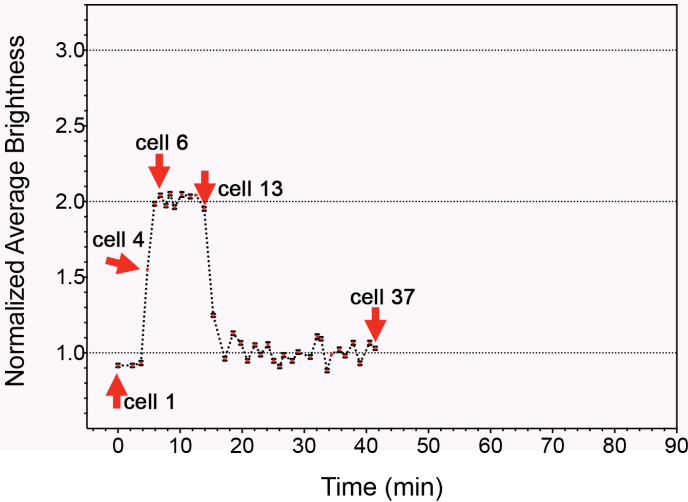


Figure 6

A



B

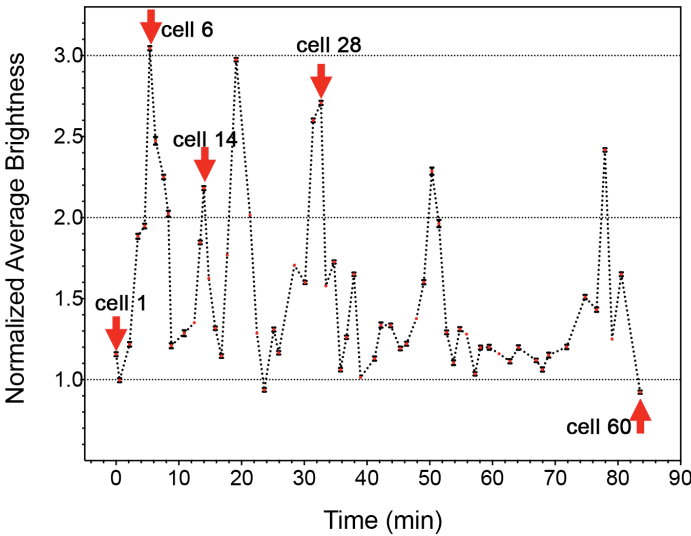
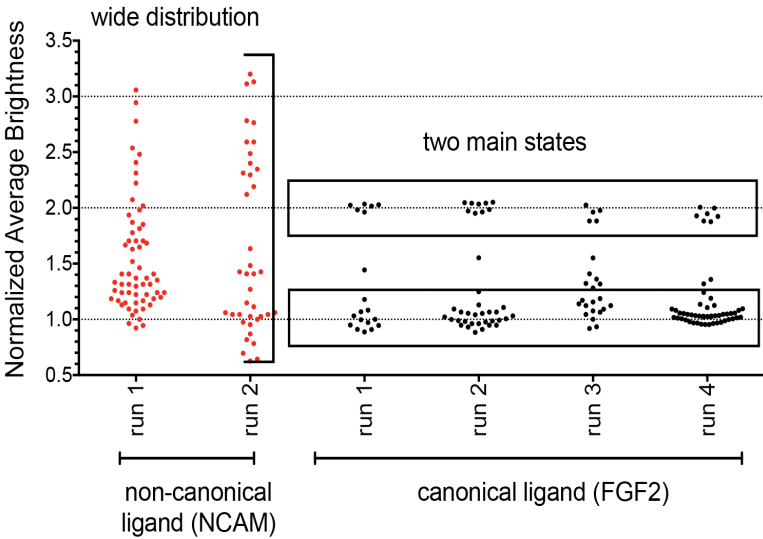
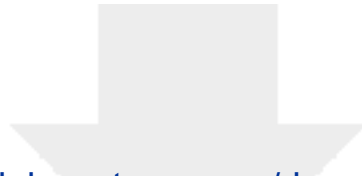




Figure 7





[Click here to access/download](#)

**Video or Animated Figure**

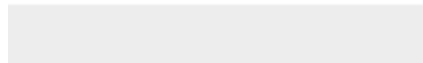
1\_HeLa\_mEGFP-FGFR1\_FGF2\_0 min.mov

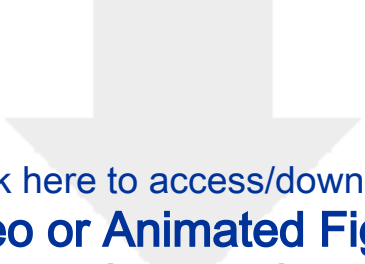




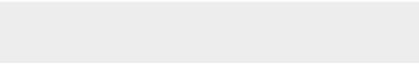

[Click here to access/download](#)

**Video or Animated Figure**  
**2\_HeLa\_GPI-mEGFP-mEGFP.mov**





Click here to access/download  
**Video or Animated Figure**  
3\_HeLa\_GPI-mEGFP.mov

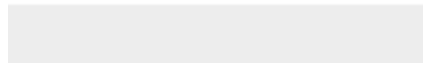




[Click here to access/download](#)

**Video or Animated Figure**

4\_HeLa\_mEGF-FGFR1\_FGF2\_7 min.mov



Parameter	GPI-mEGFP	GPI-mEGFP-mEGFP	mEGFP-FGFR1 (time = 0')	mEGFP-FGFR1 (time = 10')
Gaussian mean B-value	1.070	1.141	1.070	1.141
S.E. on the mean B-value	0.001	0.001	0.001	0.001
S.D. of the B-vauue distribution	0.059	0.067	0.077	0.075
95% Confidence interval of the mean B-value	1.069 to 1.071	1.139 to 1.143	1.069 to 1.072	1.139 to 1.143
S.D. of the 95% confidence interval of the B-value	0.058 to 0.060	0.065 to 0.069	0.075 to 0.079	0.073 to 0.078
Fitting constrain	S.D. > 0	S.D. > 0	S.D. > 0	S.D. > 0

S.E. standard error; S.D. standard deviation

Name of Material/Equipment	Company	Catalog Number	Comments/Description
3-Colour Fast TIRF Leica AM TIRF MC inverted microscope, with semi-automatic TIRF alignment. The microscope is equipped with a diode 488 nm laser, a 100x1.46 oil TIRF objective, Ex/Em Bandpass filters at 490/20 and 525/50, temperature/CO2 incubator and Andor DU 8285 VP EMCCD camera. The microscope is operated by Leica LIF software.	Leica Microsystems, Wetzlar, Germany		
Albumin from Bovine Serum 98% minimum	Sigma-Aldrich, St. Louis, MI, USA	A7906-100G	
DMEM without Phenol Red with 25 mM HEPES	GIBCO Thermo Fisher Scientific, Waltham, MA, USA	21063029	Used serum free for microscopy
DMEM high-glucose GlutaMAX I	GIBCO Thermo Fisher Scientific, Waltham, MA, USA	10566-016	Used for complete medium
Dulbecco's Phosphate Buffered Saline 10x (PBS)	Biowest, Nuaille, France	X0515-500	
Emission splitting system Photometrics DV2	TeledynePhotometrics, Tucson, AZ, USA		
Fetal Bovine Serum, qualified, Brazil	GIBCO Thermo Fisher Scientific, Waltham, MA, USA	10270106	10% inactivated supplement for complete medium
Glass bottom 35-mm sterile 1.5 dishes	MatTek, Ashland, MA, USA	P35G-0.170-14-C	uncoated, glass thickness 0.17 microns
GraphPad Prism	GraphPad Software Inc., San Diego, CA, USA		
Human cervical carcinoma (HeLa), serum-free animal component (AC) cells	Millipore-Sigma ECACC, Darmstadt, Germany	CB_08011102	
iXonEM+ 897 EMCCD (back-illuminated) ANDOR camera controlled by ANDOR Solis software	Oxford Instruments, Andor TM Technology, Abingdon-on-Thames, UK		This camera, installed in an additional port of the microscope, is used for acquiring the N&B time series
Matlab Executable N&B routine	Unit of Microscopy and Dynamic Imaging, CNIC, Madrid, Spain		download at <a href="https://www.cnic.es/en/investigacion/2/1187/tecnologia">https://www.cnic.es/en/investigacion/2/1187/tecnologia</a>
MatLab v.2018b	The MathWorks, Inc. Natick, MA, USA		<a href="https://www.mathworks.com/products/matlab.html">download at https://www.mathworks.com/products/matlab.html</a>
Penicillin:Streptomycin for tissue culture 100x	Biowhittaker Inc. Walkersville, MD, USA	LONZA 17-602E	supplement for medium at Penicillin/Streptomycin 100U/100µg.
pN1-mEGFP-FGFR1 expression vector	Unit of Gynecological Oncology Research, European Institute of Oncology IRCCS, Milan, Italy		Zamai et al., 2019
pN1-N-Gly-mEGFP-GPI expression vector	Unit of Microscopy and Dynamic Imaging, CNIC, Madrid, Spain		Hellriegel et al., 2011
pN1-N-Gly-mEGFP-mEGFP-GPI expression vector	Unit of Microscopy and Dynamic Imaging, CNIC, Madrid, Spain		Hellriegel et al., 2011
Recombinant FGF2	PeproTech EC, Ltd., London, UK		Ligand solution: 20ng/mL of FGF2 in PBS supplemented with 0.01%BSA.
Sodium pyruvate GIBCO	ThermoFisher Scientific	11360070	1mM supplement for medium
Transit-LT1 Transfection Reagent	MirusBio LLC, Madison, WI, USA	MIR 2300	
Trypsin-EDTA (0.25%), phenol red	GIBCO Thermo Fisher Scientific, Waltham, MA, USA	25200056	
Type F Immersion liquid 10 mL	Leica Microsystems, Wetzlar, Germany	11513 859	
UltraPure BSA (50 mg/mL)	ThermoFisher Scientific	AM2618	0.1% supplement for medium without phenol red used for transfections



1 Alewife Center #200  
Cambridge, MA 02140  
tel. 617.945.9051  
[www.jove.com](http://www.jove.com)

## ARTICLE AND VIDEO LICENSE AGREEMENT

Title of Article:	Oligomerization dynamics of cell surface receptors in living cells by Total Internal Reflection Fluorescence Microscopy combined with Number and Brightness analysis
Author(s):	Moreno Zamai, Antonio Trullo, Elvira Arza, Ugo Cavallaro, Valeria R. Caiolfa

Item 1: The Author elects to have the Materials be made available (as described at <http://www.jove.com/publish>) via:

☒ Standard Access

☐ Open Access

Item 2: Please select one of the following items:

☒ The Author is **NOT** a United States government employee.

☐ The Author is a United States government employee and the Materials were prepared in the course of his or her duties as a United States government employee.

☐ The Author is a United States government employee but the Materials were NOT prepared in the course of his or her duties as a United States government employee.

### ARTICLE AND VIDEO LICENSE AGREEMENT

1. **Defined Terms.** As used in this Article and Video License Agreement, the following terms shall have the following meanings: **"Agreement"** means this Article and Video License Agreement; **"Article"** means the article specified on the last page of this Agreement, including any associated materials such as texts, figures, tables, artwork, abstracts, or summaries contained therein; **"Author"** means the author who is a signatory to this Agreement; **"Collective Work"** means a work, such as a periodical issue, anthology or encyclopedia, in which the Materials in their entirety in unmodified form, along with a number of other contributions, constituting separate and independent works in themselves, are assembled into a collective whole; **"CRC License"** means the Creative Commons Attribution-Non Commercial-No Derivs 3.0 Unported Agreement, the terms and conditions of which can be found at: <http://creativecommons.org/licenses/by-nc-nd/3.0/legalcode>; **"Derivative Work"** means a work based upon the Materials or upon the Materials and other pre-existing works, such as a translation, musical arrangement, dramatization, fictionalization, motion picture version, sound recording, art reproduction, abridgment, condensation, or any other form in which the Materials may be recast, transformed, or adapted; **"Institution"** means the institution, listed on the last page of this Agreement, by which the Author was employed at the time of the creation of the Materials; **"JoVE"** means MyJoVE Corporation, a Massachusetts corporation and the publisher of The Journal of Visualized Experiments; **"Materials"** means the Article and / or the Video; **"Parties"** means the Author and JoVE; **"Video"** means any video(s) made by the Author, alone or in conjunction with any other parties, or by JoVE or its affiliates or agents, individually or in collaboration with the Author or any other parties, incorporating all or any portion

of the Article, and in which the Author may or may not appear.

2. **Background.** The Author, who is the author of the Article, in order to ensure the dissemination and protection of the Article, desires to have the JoVE publish the Article and create and transmit videos based on the Article. In furtherance of such goals, the Parties desire to memorialize in this Agreement the respective rights of each Party in and to the Article and the Video.

3. **Grant of Rights in Article.** In consideration of JoVE agreeing to publish the Article, the Author hereby grants to JoVE, subject to **Sections 4** and **7** below, the exclusive, royalty-free, perpetual (for the full term of copyright in the Article, including any extensions thereto) license (a) to publish, reproduce, distribute, display and store the Article in all forms, formats and media whether now known or hereafter developed (including without limitation in print, digital and electronic form) throughout the world, (b) to translate the Article into other languages, create adaptations, summaries or extracts of the Article or other Derivative Works (including, without limitation, the Video) or Collective Works based on all or any portion of the Article and exercise all of the rights set forth in (a) above in such translations, adaptations, summaries, extracts, Derivative Works or Collective Works and (c) to license others to do any or all of the above. The foregoing rights may be exercised in all media and formats, whether now known or hereafter devised, and include the right to make such modifications as are technically necessary to exercise the rights in other media and formats. If the "Open Access" box has been checked in **Item 1** above, JoVE and the Author hereby grant to the public all such rights in the Article as provided in, but subject to all limitations and requirements set forth in, the CRC License.



## ARTICLE AND VIDEO LICENSE AGREEMENT

4. **Retention of Rights in Article.** Notwithstanding the exclusive license granted to JoVE in **Section 3** above, the Author shall, with respect to the Article, retain the non-exclusive right to use all or part of the Article for the non-commercial purpose of giving lectures, presentations or teaching classes, and to post a copy of the Article on the Institution's website or the Author's personal website, in each case provided that a link to the Article on the JoVE website is provided and notice of JoVE's copyright in the Article is included. All non-copyright intellectual property rights in and to the Article, such as patent rights, shall remain with the Author.

5. **Grant of Rights in Video – Standard Access.** This **Section 5** applies if the "Standard Access" box has been checked in **Item 1** above or if no box has been checked in **Item 1** above. In consideration of JoVE agreeing to produce, display or otherwise assist with the Video, the Author hereby acknowledges and agrees that, Subject to **Section 7** below, JoVE is and shall be the sole and exclusive owner of all rights of any nature, including, without limitation, all copyrights, in and to the Video. To the extent that, by law, the Author is deemed, now or at any time in the future, to have any rights of any nature in or to the Video, the Author hereby disclaims all such rights and transfers all such rights to JoVE.

6. **Grant of Rights in Video – Open Access.** This **Section 6** applies only if the "Open Access" box has been checked in **Item 1** above. In consideration of JoVE agreeing to produce, display or otherwise assist with the Video, the Author hereby grants to JoVE, subject to **Section 7** below, the exclusive, royalty-free, perpetual (for the full term of copyright in the Article, including any extensions thereto) license (a) to publish, reproduce, distribute, display and store the Video in all forms, formats and media whether now known or hereafter developed (including without limitation in print, digital and electronic form) throughout the world, (b) to translate the Video into other languages, create adaptations, summaries or extracts of the Video or other Derivative Works or Collective Works based on all or any portion of the Video and exercise all of the rights set forth in (a) above in such translations, adaptations, summaries, extracts, Derivative Works or Collective Works and (c) to license others to do any or all of the above. The foregoing rights may be exercised in all media and formats, whether now known or hereafter devised, and include the right to make such modifications as are technically necessary to exercise the rights in other media and formats. For any Video to which this **Section 6** is applicable, JoVE and the Author hereby grant to the public all such rights in the Video as provided in, but subject to all limitations and requirements set forth in, the CRC License.

7. **Government Employees.** If the Author is a United States government employee and the Article was prepared in the course of his or her duties as a United States government employee, as indicated in **Item 2** above, and any of the licenses or grants granted by the Author hereunder exceed the scope of the 17 U.S.C. 403, then the rights granted hereunder shall be limited to the maximum

rights permitted under such statute. In such case, all provisions contained herein that are not in conflict with such statute shall remain in full force and effect, and all provisions contained herein that do so conflict shall be deemed to be amended so as to provide to JoVE the maximum rights permissible within such statute.

8. **Protection of the Work.** The Author(s) authorize JoVE to take steps in the Author(s) name and on their behalf if JoVE believes some third party could be infringing or might infringe the copyright of either the Author's Article and/or Video.

9. **Likeness, Privacy, Personality.** The Author hereby grants JoVE the right to use the Author's name, voice, likeness, picture, photograph, image, biography and performance in any way, commercial or otherwise, in connection with the Materials and the sale, promotion and distribution thereof. The Author hereby waives any and all rights he or she may have, relating to his or her appearance in the Video or otherwise relating to the Materials, under all applicable privacy, likeness, personality or similar laws.

10. **Author Warranties.** The Author represents and warrants that the Article is original, that it has not been published, that the copyright interest is owned by the Author (or, if more than one author is listed at the beginning of this Agreement, by such authors collectively) and has not been assigned, licensed, or otherwise transferred to any other party. The Author represents and warrants that the author(s) listed at the top of this Agreement are the only authors of the Materials. If more than one author is listed at the top of this Agreement and if any such author has not entered into a separate Article and Video License Agreement with JoVE relating to the Materials, the Author represents and warrants that the Author has been authorized by each of the other such authors to execute this Agreement on his or her behalf and to bind him or her with respect to the terms of this Agreement as if each of them had been a party hereto as an Author. The Author warrants that the use, reproduction, distribution, public or private performance or display, and/or modification of all or any portion of the Materials does not and will not violate, infringe and/or misappropriate the patent, trademark, intellectual property or other rights of any third party. The Author represents and warrants that it has and will continue to comply with all government, institutional and other regulations, including, without limitation all institutional, laboratory, hospital, ethical, human and animal treatment, privacy, and all other rules, regulations, laws, procedures or guidelines, applicable to the Materials, and that all research involving human and animal subjects has been approved by the Author's relevant institutional review board.

11. **JoVE Discretion.** If the Author requests the assistance of JoVE in producing the Video in the Author's facility, the Author shall ensure that the presence of JoVE employees, agents or independent contractors is in accordance with the relevant regulations of the Author's institution. If more than one author is listed at the beginning of this Agreement, JoVE may, in its sole

## ARTICLE AND VIDEO LICENSE AGREEMENT

discretion, elect not take any action with respect to the Article until such time as it has received complete, executed Article and Video License Agreements from each such author. JoVE reserves the right, in its absolute and sole discretion and without giving any reason therefore, to accept or decline any work submitted to JoVE. JoVE and its employees, agents and independent contractors shall have full, unfettered access to the facilities of the Author or of the Author's institution as necessary to make the Video, whether actually published or not. JoVE has sole discretion as to the method of making and publishing the Materials, including, without limitation, to all decisions regarding editing, lighting, filming, timing of publication, if any, length, quality, content and the like.

12. **Indemnification.** The Author agrees to indemnify JoVE and/or its successors and assigns from and against any and all claims, costs, and expenses, including attorney's fees, arising out of any breach of any warranty or other representations contained herein. The Author further agrees to indemnify and hold harmless JoVE from and against any and all claims, costs, and expenses, including attorney's fees, resulting from the breach by the Author of any representation or warranty contained herein or from allegations or instances of violation of intellectual property rights, damage to the Author's or the Author's institution's facilities, fraud, libel, defamation, research, equipment, experiments, property damage, personal injury, violations of institutional, laboratory, hospital, ethical, human and animal treatment, privacy or other rules, regulations, laws, procedures or guidelines, liabilities and other losses or damages related in any way to the submission of work to JoVE, making of videos by JoVE, or publication in JoVE or elsewhere by JoVE. The Author shall be responsible for, and shall hold JoVE harmless from, damages caused by lack of sterilization, lack of cleanliness or by contamination due to

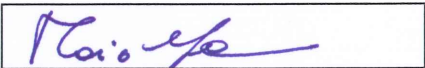
the making of a video by JoVE its employees, agents or independent contractors. All sterilization, cleanliness or decontamination procedures shall be solely the responsibility of the Author and shall be undertaken at the Author's expense. All indemnifications provided herein shall include JoVE's attorney's fees and costs related to said losses or damages. Such indemnification and holding harmless shall include such losses or damages incurred by, or in connection with, acts or omissions of JoVE, its employees, agents or independent contractors.

13. **Fees.** To cover the cost incurred for publication, JoVE must receive payment before production and publication the Materials. Payment is due in 21 days of invoice. Should the Materials not be published due to an editorial or production decision, these funds will be returned to the Author. Withdrawal by the Author of any submitted Materials after final peer review approval will result in a US\$1,200 fee to cover pre-production expenses incurred by JoVE. If payment is not received by the completion of filming, production and publication of the Materials will be suspended until payment is received.

14. **Transfer, Governing Law.** This Agreement may be assigned by JoVE and shall inure to the benefits of any of JoVE's successors and assignees. This Agreement shall be governed and construed by the internal laws of the Commonwealth of Massachusetts without giving effect to any conflict of law provision thereunder. This Agreement may be executed in counterparts, each of which shall be deemed an original, but all of which together shall be deemed to be one and the same agreement. A signed copy of this Agreement delivered by facsimile, e-mail or other means of electronic transmission shall be deemed to have the same legal effect as delivery of an original signed copy of this Agreement.

A signed copy of this document must be sent with all new submissions. Only one Agreement is required per submission.

### CORRESPONDING AUTHOR

Name:	Valeria R Caiolfa	
Department:	Centro di Imaging Sperimentale	
Institution:	Ospedale San Raffaele, Via Olgettina 58, 20132 Milano, Italy	
Title:	Dr.	
Signature:		Date: June 4 <sup>th</sup> - 2019

Please submit a **signed** and **dated** copy of this license by one of the following three methods:

1. Upload an electronic version on the JoVE submission site
2. Fax the document to +1.866.381.2236
3. Mail the document to JoVE / Attn: JoVE Editorial / 1 Alewife Center #200 / Cambridge, MA 02140

### **Reply to the Editorial Comments:**

- Please take this opportunity to thoroughly proofread the manuscript to ensure that there are no spelling or grammatical errors.
- **Textual Overlap:** Significant portions show significant overlap with previously published work. Please re-write the text on lines 43-50, 73-75, 81-119, 140- 145, 158-165, 468-473 to avoid this overlap.  
We have rephrased the lines (highlighted in blue font colour).
- **Protocol Detail:** Please note that your protocol will be used to generate the script for the video, and must contain everything that you would like shown in the video. **Please add more specific details (e.g. button clicks for software actions, numerical values for settings, etc) to your protocol steps.** There should be enough detail in each step to supplement the actions seen in the video so that viewers can easily replicate the protocol.  
1) 3.2, 3.3: Mention explicit details of software actions.  
We provide a link for downloading the software
- **Protocol Highlight:** Please ensure that the highlighting is continuous and does not exceed 2.75 pages.  
The limits are fulfilled
- **Discussion:** JoVE articles are focused on the methods and the protocol, thus the discussion should be similarly focused. Please ensure that the discussion covers the following in detail and in paragraph form (3-6 paragraphs): 1) modifications and troubleshooting, 2) limitations of the technique, 3) significance with respect to existing methods, 4) future applications and 5) critical steps within the protocol.  
We think we fulfil all these requirements
- **References:** Please spell out journal names.  
For the reference list we have applied in EndNote the style downloadable for JoVE web site, according to the link provided by your editorial office.
- **Commercial Language:** JoVE is unable to publish manuscripts containing commercial sounding language, including trademark or registered trademark symbols (TM/R) and the mention of company brand names before an instrument or reagent. Examples of commercial sounding language in your manuscript are GlutaMAX, GIBCO, MirusBio LLC, Translt-LT1, Photometrics DV2, etc  
1) Please use MS Word's find function (Ctrl+F), to locate and replace all commercial sounding language in your manuscript with generic names that are not company-specific. All commercial products should be sufficiently referenced in the table of materials/reagents. You may use the generic term followed by "(see table of materials)" to draw the readers' attention to specific commercial names.  
All commercial language has been removed
- If your figures and tables are original and not published previously or you have already obtained figure permissions, please ignore this comment. If you are re-using figures from a previous publication, you must obtain explicit permission to re-use the figure from the previous publisher (this can be in the form of a letter from an editor or a link to the editorial policies that allows you to re-publish the figure). Please upload the text of the re-print permission (may be copied and pasted from an email/website) as a Word document to the Editorial Manager site in the "Supplemental files (as requested by JoVE)" section. Please also cite the figure appropriately in the figure legend, i.e. "This figure has been modified from [citation]."  
We include in the submission of the revised manuscript the explicit permission of Journal Cell Science to partially reproduce some illustration. We have amended the figure legends accordingly.

**From:** permissions permissions@biologists.com  
**Subject:** RE: Zamai et al Journal of Cell Science(2019), 132 doi:10.1242/jcs.220624  
**Date:** 12 July 2019 at 15:10  
**To:** Caiolfa Valeria caiolfa.valeria@hsr.it, permissions permissions@biologists.com  
**Cc:** Moreno Zamai mzamai@cnic.es

P

Dear Valeria,

Thank you for your request. Permission for authors re-use is granted automatically.

The acknowledgement is important and should state "reproduced/adapted with permission" and give the source journal name - the acknowledgement should either provide full citation details or refer to the relevant citation in the article reference list - the full citation details should include authors, journal, year, volume, issue and page citation.

Where appearing online or in other electronic media, a link should be provided to the original article (e.g. via DOI).

Journal of Cell Science: <http://www.biologists.com/journal-of-cell-science>

We wish you the best of luck with your manuscript.

Kind regards

Richard

**Richard Grove**  
Commercial Manager  
The Company of Biologists Ltd  
Bidder Building, Station Road, Histon, Cambridge, CB24 9LF, UK  
T: +44 (0) 1223 632 850 [richard.grove@biologists.com](mailto:richard.grove@biologists.com) | [www.biologists.com](http://www.biologists.com)

---

Registered office: The Company Of Biologists Ltd, Bidder Building, Station Road, Histon, Cambridge CB24 9LF, United Kingdom, Registered in England and Wales. Company Limited by Guarantee No 514735. Registered Charity No 277992 The information contained in this message and any attachment is confidential, legally privileged and is intended for the addressee only. Any dissemination, distribution, copying, disclosure or use of this message/attachment or its contents is strictly prohibited and may be unlawful. No contract is intended or implied, unless confirmed by hard copy. If you have received this message in error, please inform the sender and delete it from your mailbox or any other storage mechanism. The Company of Biologists Ltd cannot accept liability for any statements made which are clearly the senders' own and not expressly made on behalf of The Company of Biologists Ltd or one of their agents.

---



Reviewer #1:

Manuscript Summary:

This protocol describes the use of TIRF microscopy and moment analysis (N&B) for the quantification of protein multimerization in living cells. As a practical example, the dimerization of FGFR1 induced by ligand addition is described.

I found the technical approach interesting and the manuscript well-written. My major concern (see below for details) is that the protocol seems written for somebody who already has an idea of what has to be done, does not need to change or tune any condition and will use the same hardware. Nothing wrong with this but, in my understanding, the authors have here the chance to discuss the protocol in a deeper way, while also making it more approachable for new-users or users who do not work with the same hardware. We thank the reviewer for the careful and constructive revision of our manuscript. We agree with the general comment. Accordingly, we have revised the text to keep it in the length limits but, at the same time, to present a protocol less linked to the specific microscope available to us and to our model sample, with the intention of providing a guide more generally applicable by non-expert users. For this reason, we have revised the figure legends in depth. Major changes are highlighted in blue text font. Our replies to the specific comments are reported below (in blue font).

More specifically,

Major Concerns:

1- What camera is used here?

We have realized that there has been some confusion in the protocol about the use of the two cameras installed on our commercial TIRF microscope. We have carefully revised the entire TIRF section in the protocol, the legend of Figure 1 and amended the Table of Materials. The camera used for acquiring the N&B series is a iXon897 EMCCD by Andor TM Technology.

2- What are the advantages of using EMCCD vs e.g. sCMOS? Would sCMOS create trouble if one wanted to look at the moments of spatial distributions, rather than within single pixels?

EMCCD cameras have an extended multiplication register that amplifies the photoelectron signal before readout, thus, sensitivity increases two or three order of magnitude without increasing the read noise. EMCCD cameras fit well into low-light applications requiring also a moderate to high frame-rate as in case of N&B time series. More importantly, however, are the characteristics of the camera noise. Noise in scientific EMCCD and CCD cameras is generally random, following a Gaussian distribution. Read noise, photon shot noise and dark current noise follow Gaussian-type distributions. Scientific CMOS cameras have distributions of read noise across the pixels that are highly skewed outside the Gaussian distribution towards higher noise values. The skewed distribution indicates that a relevant number of pixels have a variety of noise levels and that noise is not random in the image. N&B can be applied only if the detector noise is random. The point raised by the Reviewer is important for the protocol, therefore we have included a comment in the revised legend of Figure 1 (lines 437-438).

Honestly, we are not very familiar with moments of spatial distributions, but we guess that non Gaussian noise in the images might not be optimal for the approach.

3-Does the EM value just affect the factor G or also the measurement in general (I understand that the very last question might be outside the scope though).

Yes, it does, changing the S/N. Therefore, we keep EM constant and at the highest value. We follow the method implemented by Unruh, J. R. & Gratton (2008) for EMCCD cameras in which the calibration is made a part, running a black time series alone. Since we measure the calibration parameters simultaneously to the acquisition of each time series, we could even change the EM value, but it wouldn't be recommended.

4- What is the role of pixel size (does it have to be e.g. smaller than the PSF)?

Yes, pixel size must be smaller than the PSF to avoid artifacts due to inhomogeneity of the illumination that causes extra variance.

5- Can a volume be calibrated so to obtain absolute concentrations?

Yes, volume can be calibrated for obtaining absolute concentrations. Due to the length limits of the text, we don't have room in this protocol to consider the computation of the average number of molecule ("N") and the analytical approach for the volume calibration.

6- What is the advantage of N&B in TIRF geometry, compared other excitation/detection schemes?

N&B runs equally well with confocal laser scanning microscopes equipped with continuous wave or pulsed single photon lasers or multiphoton microscopes, and with analogue or photon counting detectors. The inverted objective-based TIRF geometry is preferred for studying proteins at the plasma membrane and at the cell adhesion sites because the evanescent illumination, which decreases exponentially from the cover slip, doesn't penetrate the cell more than 70-250 nm adjacent to the coverslip. We have revised Figure 3 and the legend to clarify these concepts.

7- What is the influence of the pixel dwell time / frame rate?

We thank the Reviewer for this important question that we didn't discuss in the first version of the manuscript. Now we have inserted a new paragraph in the discussion dealing with these concepts (lines 628-648).

8- Using very fast acquisition, like the one described here (1 ms), wouldn't one see the effect of fast photophysics (e.g. blinking) in fluctuations as well?

Blinking of mEGFP is in the 1-10 microsec range, our exposure time is 1 ms. In this condition blinking shouldn't affect the measurement.

9- Of course, the accumulation time is not that important, as long as it stays smaller than typical diffusion times, but what is the time between frames? This might be discussed better.

The Reviewer's comments here and in point 7 about time scales are important and, as it is said above, we have introduced a dedicated paragraph in the discussion (lines 628-648).

10- I completely missed the reason/use of the two cameras. Are two cameras needed?

We apologize again for the confusion about the two cameras. We have realized that this was a weak part of the protocol and, as it is said above, we have revised the entire TIRF section and explained the reason of our specific configuration in the legend of Figure 1 (lines 424-436). Two cameras are not needed if the proper exposure and cycle times can be obtained with the microscope built-in camera.

11- Lines 273-275: I understand the author refer to a specific software, but maybe they can explain a bit better what happens during these steps, also for non-expert users or for users working with other setups (I understand that this is rather a "style choice" ). Some things can definitely be generalized though (e.g. GFP filter cube)

We have revised the entire TIRF section of the protocol to make the protocol more general and approachable by non-expert users.

12- Lines 281-282:

similar to the previous point. Why 110 nm? What happens if this number is varied?

Evanescent wave penetration is addressed in the revised legend of Figure 3 (lines 484-492).

13- What if the software does not have this button? Maybe a hint to users who have to manually change the angle and a reference to papers describing how to measure the penetration depth might be useful. Or some hint from the authors might suffice. At this regard, Figure 3 C and D should be explained and discussed in more detail.

We have revised Figure 3 legend in points C and D (lines 493-501) and added two references for angle calibration (refs Burghardt 2012 and Gell et al., 2009).

14- Is it possible to measure also at non-optimal depth?

Yes. However, non-optimal depth means that if you go too deep inside the cell you might get relevant signal from intracellular structures and vesicles and autofluorescence. If the section is too tiny, S/N might be too low when you run the series at the shortest exposure time. This point is now better discussed in the revised Figure 3 legend point B (lines 484-501).

15- What are the laser powers used (e.g. at the objective lens)?

The objective lens is specified in the Table of Materials, 100x1.46 oil and in the legend of Figure 1 (line 425). The laser power is now specified in the revised protocol (now line 280-281).

And, very important, when an user is calibrating the instrument at the beginning: what kind of signal can be expected for a certain molecule at a certain laser power?

Well, here the answer cannot be specific. We might say that one can get a rough idea of the S/N of the first frame of the first series to evaluate both, the laser power and the expression of the fluorescent construct in the chosen cell.  $S/N \geq 2$  might be a starting condition. We have inserted this guideline in the protocol (lines 287-289).

I understand that one could compare the final B values to those reported here, but is there a simple way for checking at the beginning of the measurement that the setup is working in an optimized way?

The calibration of the TIRF angle is independent of the subsequent measurement. Nowadays, commercial TIRF microscopes have thorough automatic routines that are self-checking. Depth and orientation of the evanescent wave is more subjective. However, we can only give general guidelines because signal is a function of several parameters that can change a lot from one equipment to another depending on the type of laser, quality of the objective (not only magnification and NA), type and quality of filters, type and quality of the camera. At the end, as we stress in the manuscript, it is of foremost importance to have a reference sample that can be explored at different expression levels of the reference fluorescent protein construct.

16- Line 316: Can N (or the intensity) be too high (for statistics, S/N or the hardware)?

Yes it can. However, N&B is less restrictive than PCH/FCS and it covers a wider range of fluorophore concentrations. The lowest limit depends on S/N. Statistics becomes a problem for  $S/N < 2$  (we have amended the text for this (see lines 282-286). EMCCDs are more sensitive at low-light level applications than CCD or scientific CMOS cameras. The highest limit mainly depends on the dynamic range of the camera that needs operate at the highest EM gain. Generally, the highest limit depends on the expression levels in sample. Saturation of the detector must be avoided, and in this sense, very bright clusters scattered in a dim cell area often might not be analyzed. N&B is still an approach for low-intensity signals.

17- Line 523: The authors report the widths of the B distributions. What is the physical meaning of this width? It sounds interesting but I am not sure about its use. In spatially inhomogeneous samples, I imagine it says something about the inhomogeneity. But what about homogeneous samples? Is it connected to S/N? The smaller, the better?

Since we do not observe bimodal or multimodal frequency distributions, we conclude that samples are homogeneous. This means that we cannot distinguish significant areas (1000 pixels at least, as from our previous work in Hellriegel et al., 2011, supplemental figures S1-S4) that are associated with statistically different brightness. Therefore, we think that the width of the distributions mainly depends on the S/N. We work at the limit of S/N to avoid over expression of the receptor in the membrane, while we generally accept higher expression levels of the reference constructs that do not cluster and that we have repeatedly studied also in FCS. The reference samples have better S/N and narrower distribution width. In addition, we also think that the width of the distributions can be associated to minor environmental changes affecting the brightness of the fluorophore. The fitting parameters of supplemental table describe the overlap of the monomer and dimer distributions and, thus, the confidence limit of the measurements. As we showed in our previous work, the width of the distribution also depends on the number of frames in the time sequence (more frames, better statistics) and on the diffusion coefficient (supplemental figures in Hellriegel et al., 2011).

18- I was surprised to see that GFP dimers had indeed a brightness 2 times higher than the monomer. How do the authors explain it in the light of published observations regarding the presence of an offset in the linear relation between number of subunits and brightness (Slaughter et al 2008 PlosONE) or, using a

different physical model, a <100% fluorescence probability for GFP (Ulbrich et al 2007 Nature Methods, Dunsing et al 2018 Scientific Reports, Godin et al 2015 BiophysJ)?

Figure 5B in Slaughter et al 2008 PlosONE paper shows an offset due to autofluorescence. In TIRF the autofluorescence contribution to signal is minimized since the exponential decay of the evanescent wave excludes the excitation of the cell interior. Ulbrich et al 2007 Nature Methods does not apply fluctuation methods but single molecule photobleaching. The paper published by Dunsing et al in Scientific Reports 2018 is very interesting. However, the dark states are much less critical for mEGFP than for mEYFP and mCherry. Moreover, in that work N&B is applied to laser scanning confocal images at a pixel dwell time of 25 microsec, 40 times faster than our exposure time, because they track faster diffusion times. Thus, long-lived dark states might not affect our measurements of plasma membrane proteins, which we can follow with longer dwell times. Obviously, a part from the example shown in this manuscript, we have about 10% variability on the brightness of the reference dimer, more than what we observe for the monomeric brightness (Zamai et al., 2019). Finally, although the emission probability for each fluorescent protein is considered less than 100 %, the deviation from linearity might be hidden by the relatively large distribution width of our data.

Minor Concerns:

19- Figure 1 could be explained better for non-expert users.  
The legend has been re-written including more details.

20- Lines 89-94: spIDA should also be mentioned  
Undoubtedly, SpIDA must be mentioned. We apologize for having neglected this very useful approach. We have added a sentence with reference (lines 79-83).

21- Line 172: I do not understand the "For that" here. The difference between epsilon and B (or the definition of B itself) do not "require" the existence of a subpopulation of immobile fluorophores. The physical reason is rather the poissonian nature of the photon detection process. But I might have just misunderstood what the authors meant here.  
We have revised the text (lines 178-179).

22- Line 246: something is wrong here WHY?  
We have deleted the note that did not make much sense.

23- Line 260: why both lamp and laser?  
We use the lamp simply because using an excitation bandpass filter we have more light on sample. It is easier to inspect the dish quickly and select a cell with dim-medium fluorescence. We added a note that this step can also be done with laser illumination (lines 253-254).

24- New cameras work in photon counting mode. How would this affect the described approach? Photon counting mode with background is equivalent to analog mode with  $S=1$  and with  $\sigma_d^2$  and offset measured in the same way as for an analog system [Dalal et al., Micros Res Tech 2008]. We have introduced this comment in the revised Figure 4 legend (lines 520-522).

25- Line 438: The dimerization is described as a "slow process" but, for example, it seems very quick in Fig 6A. Can the process be actually followed in between cells with only monomers and cells with 100% dimers?

The process from monomers to dimers takes about 2 minutes (in terms of cell processes it is quite slow). However, we could capture intermediate states (a mixture between monomers and dimers) as in cell 4 of Fig 6A. Because of the technical constraints (search a new cell at each time point, optimize focus, activate the camera) it is impossible to collect two images from two different cells in less than one minute.

26- Figure 4B: Is there a specific reason for the shape and number of the calibration ROIs?  
The shape is due only to the type of dual view adaptor that we can use. The number of pixels cannot be less than 1000 for statistics [Hellriegel et al., 2011, supplemental figures].



27- Line 470: The signal does fluctuate also in this case  
The figure 2 legend is amended (lines 455-456).

28- Line 474: "equal number of molecules" might not be clear  
The figure 2 legend is amended (now lines 458-460).

29- Line 505: it might useful to some reader if the authors explained how S is in practice connected to the single photon response  
This has been specified in the revised text (line 202).

## Reply to Reviewer #2:

### Manuscript Summary:

The authors describe a protocol for measurement of membrane receptor oligomerization dynamics in live cells using N&B, TIRF microscopy and a custom software. The manuscript goes in the step-by-step experimental process from sample preparation to setting TIRF microscope and camera for acquisition. The approach for dynamics here presented uses different cells for each aggregated time-point, where each measurement consists of a number (500-700) of frames, from which one average value of Brightness is calculated. Calibration is performed on an image-to-image basis by intentionally covering part of the sensor, thus allowing for a measurement of the background parameters for each image.

We thank the reviewer for the careful and constructive revision of our manuscript.

Our replies to his individual comments are reported below (in blue font). We have modified the manuscript also to comply with Editor's requests and Reviewer # 1 comments. Accordingly, we have revised the protocol section to keep it in the length limits. At the same time to be less linked to the specific microscope available to us and to our particular biological sample, we have inserted more details in the figure legends, with the intention of providing a guide more generally applicable by non-expert readers. Major changes of the text are highlighted in blue font.

### Major Concerns:

The article is well written and detailed in the experimental and imaging settings. I don't have major concerns regarding the protocol, just minor concerns regarding the specific values (for example exposure, number of frames) which are named in some of the protocol's steps.

Minor Concerns: I have a few minor concerns which I believe could help improve the manuscript.

1. line 92 of introduction, in the section describing FCS and PCH, it would be helpful for a reader to mention Scanning FCS which, while also limited in the capability of imaging large areas, can cover smaller areas larger than a single-point quite efficiently. The work of Elizabeth Hinde (Quantifying the dynamics of the oligomeric transcription factor STAT3 by pair correlation of molecular brightness. Nature Communications 2016; 7(11047). ) would be a good example to reference.

As suggested, we have introduced scanning FCS. In addition to the interesting work by Hinde, we have also mentioned the original paper by Levi V., et al., 2003 that introduced the approach and a 2018 methodological reference.

2. line 249, TIRF Imaging 2.1.2 , "wait for camera to cool down" probably should be changed to "wait for camera to reach a stable temperature".

We have changed the sentence in "wait for the camera to reach the proper working temperature" and added a NOTE (lines 245-247).

3. line 274 TIRF Imaging 2.1.7 ""Contrast Method" to the " TIRF Mthod"" the authors should mention here, not only in the note below, that these two methods might have different names on different systems.

We have revised the test (lines 258-259).

4. line 286 TIRF Imaging 2.2.1 the authors could mention briefly how the exposure time is chosen for this camera. On a different note, this step of the process appears very specific for the instrument used by the authors. Is the instrument custom made or commercially available? Some details can be found in the table at the end of the manuscript but it would be helpful to know some of the essential requirements before the start of the protocol steps. In this case the step appears to require an Andor camera and Andor's Solis software, independently from the Leica instrument.

We have realized that this was a weak part of the protocol and we have revised the entire TIRF section, revised figure 1 and 3 in depth, and dedicated a new paragraph in the discussion to the topic of exposure and cycling times.

5. line 296 TIRF Imaging 2.2.3 how were exposure and gain chosen here? are they specific for the membrane receptor used in this experiment? Should exposure be dependent on the diffusion rate of the labelled receptor?

See the revised sections mentioned above. We have chosen the exposure time of 1 ms accordingly with the diffusion rate of labelled receptors in the plasma membrane. The EMgain =1000 is the highest value for the Andor camera at our disposal, and it is the value suggested by Unruh and Gratton (Unruh, J. R. & Gratton, E. Analysis of molecular concentration and brightness from fluorescence fluctuation data with an electron multiplied CCD camera. *Biophys J.* **95** (11), 5385-5398, (2008).)

6. line 322 TIRF Imaging 2.2.8 would it be more efficient to pick cells for imaging (and save corresponding positions) before adding ligand?

Many motorized stages allow for saving positions, this would ensure a more constant time between the image-series on different cells.

We have added this option in the revised text (lines 312-314).

7. line 488 Figure 3 caption: SW should be spelled out once in this paragraph for ease of reading.

Amended

8. there is a reference for N&B GUI Matlab routine (Zamai et al, 2019), however given the software is essential for this protocol it would be helpful to have a link in this manuscript (for example a webpage or cloud-storage link) where to obtain the analysis tool.

We have made our routine available and inserted a direct link for download (lines 327-328).

Figure S1

